JOURNAL OF GEOPHYSICAL RESEARCH, VOL. 115, B12422, doi:10.1029/2009JB006789, 2010

Paleoseismological evidence of surface faulting along the northeastern Himalayan front, India: Timing, size, and spatial extent of great earthquakes

Senthil Kumar,[1] Steven G. Wesnousky,[2] R. Jayangondaperumal,[3] T. Nakata,[4] Y. Kumahara,[5] and Vimal Singh[1,6]

Received 15 July 2009; revised 10 April 2010; accepted 27 May 2010; published 29 December 2010.

[1] The ~2500 km long Himalayan arc has experienced three large to great earthquakes of M_w 7.8 to 8.4 during the past century, but none produced surface rupture. Paleoseismic studies have been conducted during the last decade to begin understanding the timing, size, rupture extent, return period, and mechanics of the faulting associated with the occurrence of large surface rupturing earthquakes along the ~2500 km long Himalayan Frontal Thrust (HFT) system of India and Nepal. The previous studies have been limited to about nine sites along the western two-thirds of the HFT extending through northwest India and along the southern border of Nepal. We present here the results of paleoseismic investigations at three additional sites further to the northeast along the HFT within the Indian states of West Bengal and Assam. The three sites reside between the meizoseismal areas of the 1934 Bihar-Nepal and 1950 Assam earthquakes. The two westernmost of the sites, near the village of Chalsa and near the Nameri Tiger Preserve, show that offsets during the last surface rupture event were at minimum of about 14 m and 12 m, respectively. Limits on the ages of surface rupture at Chalsa (site A) and Nameri (site B), though broad, allow the possibility that the two sites record the same great historical rupture reported in Nepal around A.D. 1100. The correlation between the two sites is supported by the observation that the large displacements as recorded at Chalsa and Nameri would most likely be associated with rupture lengths of hundreds of kilometers or more and are on the same order as reported for a surface rupture earthquake reported in Nepal around A.D. 1100. Assuming the offsets observed at Chalsa and Nameri occurred synchronously with reported offsets in Nepal, the rupture length of the event would approach 700 to 800 km. The easternmost site is located within Harmutty Tea Estate (site C) at the edges of the 1950 Assam earthquake meizoseismal area. Here the most recent event offset is relatively much smaller (<2.5 m), and radiocarbon dating shows it to have occurred after A.D. 1100 (after about A.D. 1270). The location of the site near the edge of the meizoseismal region of the 1950 Assam earthquake and the relatively lesser offset allows speculation that the displacement records the 1950 M_w 8.4 Assam earthquake. Scatter in radiocarbon ages on detrital charcoal has not resulted in a firm bracket on the timing of events observed in the trenches. Nonetheless, the observations collected here, when taken together, suggest that the largest of thrust earthquakes along the Himalayan arc have rupture lengths and displacements of similar scale to the largest that have occurred historically along the world's subduction zones.

Citation: Kumar, S., S. G. Wesnousky, R. Jayangondaperumal, T. Nakata, Y. Kumahara, and V. Singh (2010), Paleoseismological evidence of surface faulting along the northeastern Himalayan front, India: Timing, size, and spatial extent of great earthquakes, *J. Geophys. Res.*, *115*, B12422, doi:10.1029/2009JB006789.

[1]Centre for Earth Sciences, Indian Institute of Science, Bangalore, India.
[2]Center for Neotectonic Studies, University of Nevada, Reno, Nevada, USA.
[3]Wadia Institute of Himalayan Geology, Dehradun, Uttaranchal, India.
[4]Department of Geography, Hiroshima Institute of Technology, Hiroshima, Japan.
[5]Faculty of Education, Gunma University, Gunma, Japan.
[6]Presently at Department of Geology, Center for Advanced Study, University of Delhi, Delhi, India.

0148-0227/10/2009JB006789

1. Introduction

[2] The Himalayan collision started about 50–55 Myr ago and has given rise to the highest mountains on Earth [*Avouac and Tapponnier*, 1993; *Harrison et al.*, 1992; *Molnar and Tapponnier*, 1975; *Tapponnier et al.*, 2001] (Figure 1). The rate of convergence subsequent to the collision between India and stable Eurasia has continued at a rate of about 38–50 mm/yr [*Banerjee and Bürgmann*, 2002; *Bilham et al.*, 1997; *Bilham et al.*, 1998; *DeMets et al.*, 1994; *Patriat and Achache*, 1984; *Paul et al.*, 2001]. The convergence has been accommodated primarily by thrust fault systems and a combination of lateral extrusion and crustal thickening in the high Tibetan plateau to the north [*Larson et al.*, 1999; *Molnar and Tapponnier*, 1975]. From north to south, the three thrust systems are the Main Central Thrust (MCT), the Main Boundary Thrust (MBT), and the Himalayan Frontal Thrust (HFT) (Figure 1). It is generally considered that the three thrust fault systems reflect a southward migration of the Himalayan front through time [*Gansser*, 1964; *Le Fort*, 1975; *Nakata*, 1972, 1989; *Valdiya*, 1992; *Yeats et al.*, 1992], and that each of the faults sole into the same major mid-crustal décollement, the Main Himalayan Thrust (MHT) [*Nelson et al.*, 1996; *Pandey et al.*, 1995; *Schelling and Arita*, 1991; *Seeber and Armbruster*, 1981; *Zhao et al.*, 1993] (Figure 1). Of the three thrust fault systems, the southernmost and present-day active deformation front is marked by the Himalayan Frontal Thrust (HFT), also frequently referred to as Main Frontal Thrust (MFT) [*Nakata*, 1972, 1989].

[3] Plate motion models [*DeMets et al.*, 1994; *Treloar and Coward*, 1991], geologic observations [*Kondo et al.*, 2008; *Kumar et al.*, 2001; *Kumar et al.*, 2006; *Lavé and Avouac*, 2000; *Lavé et al.*, 2005; *Nakata et al.*, 1998; *Upreti et al.*, 2000; *Wesnousky et al.*, 1999; *Yule et al.*, 2006], and GPS measurements [*Bilham et al.*, 1997; *Paul et al.*, 2001; *Wang et al.*, 2001] indicate that ~10–20 mm/yr of the total 40–50 mm/yr of relative convergence between stable India and Eurasia is absorbed by faulting and folding along the HFT (Figure 1). Instrumental seismicity, geodetic monitoring, and the rupture extent of historical earthquakes provide evidence that the great Himalayan earthquakes nucleate below the high Himalaya along the MHT and propagate southward along the décollement [e.g., *Nelson et al.*, 1996; *Nelson*, 1998; *Pandey et al.*, 1995; *Seeber and Armbruster*, 1981]. Historical earthquakes attributed to slip on the MHT are the 1505 central Himalayan earthquake (M_w ~ 8.2), the 1555 Kashmir earthquake (M_w ~ 7.6), the 1803 Kumaon-Garhwal earthquake (M_w ~ 7.5), the 1833 Nepal earthquake (M_w ~ 7.3), the 1905 Kangra earthquake (M_w ~ 7.8), the 1934 Bihar-Nepal earthquake (M_w ~ 8.1), and the 1950 Assam earthquake (M_w ~ 8.4) [*Ambraseys and Bilham*, 2000; *Ambraseys and Jackson*, 2003; *Ambraseys and Douglas*, 2004; *Bilham*, 1995; *Bilham*, 2004; *Bilham and Ambraseys*, 2005; *Chander*, 1989; *Martin and Szeliga*, 2010; *Molnar and Pandey*, 1989; *Pandey and Molnar*, 1988; *Szeliga et al.*, 2010; *Wallace et al.*, 2005] (Figure 1).

[4] A decade of paleoseismological investigations in the Himalaya has been driven by the lack of recognized surface rupture associated with the largest of the historical earthquakes and the quest to understand the relationship between strain accumulation and strain release associated with the Earth's largest continental thrust system. During that time, numerous paleoseismological studies employing trenches excavated across scarps of the HFT have been conducted in an effort to understand the timing, size, rupture extent, return period, and mechanics of the faulting associated with large to great Himalayan earthquakes [*Kondo et al.*, 2008; *Kumar et al.*, 2001; *Kumar et al.*, 2006; *Lavé et al.*, 2005; *Malik and Nakata*, 2003; *Nakata et al.*, 1998; *Oatney et al.*, 2001; *Upreti et al.*, 2000; *Yule et al.*, 2006]. The studies have been limited primarily to the western two-thirds of the HFT, extending through northwest India and along the southern border of Nepal. Here we present the results of paleoseismic investigations at three additional sites farther to the northeast along the HFT within the Indian states of West Bengal and Assam. The three sites, located near the village of Chalsa, the Nameri Tiger Preserve, and within the Harmutty Tea Estate, are located between the meizoseismal areas of the 1934 Bihar-Nepal and 1950 Assam earthquakes (Figure 1 and sites A, B, and C, respectively, in Figure 2). Results from the trench studies are then combined with prior paleoseismological studies reported to the west and with the historical earthquake record to illustrate the timing and spatial extent of large to great earthquakes along the HFT.

2. Methods

[5] We mapped geomorphic surfaces at each site using Shuttle Radar Topographic Mission (SRTM) imagery downloaded from the Global Land Cover Facility web site (http://glcf.umiacs.umd.edu/data/srtm/). The details of each site location (sites A, B, and C in Figure 2), surficial mapping (Figures 3, 7, and 10), and the results of available radiocarbon dating are provided in section 3. For each site, we measured profiles across fault scarps that offset the youngest geomorphic surfaces. Trenches were then excavated across the active fault scarps preserved in Holocene alluvial/fluvial sediments. Trench exposures were logged to show the structural and stratigraphic relations used to determine the timing, geometry, and size of past earthquakes. Fault traces and stratigraphic contacts were logged in the field using a 1 m or 2 m grid system on the exposure faces depending on the amount of detail necessary to illustrate the stratigraphic contacts and fault traces. All measurements discussed in trench descriptions are in meters along the length of the trench from north to south or east to west, followed by depth below in meters relative to an arbitrary datum established near the top of the north or east end of the trench. The sediments observed in the trench exposure were differentiated as individual units on the basis of degree of soil development, grain size, texture, color, bioturbation, lithology, and inferred depositional environment. These units are numbered in increasing order from oldest to youngest in the trench log. Radiocarbon (^{14}C) determined accelerator mass spectrometer ages of detrital charcoal collected from the trenches are used to constrain the age of the stratigraphic units exposed in the trenches and hence the age of past earthquake events along the HFT (Tables 1–3). All ages reported are 2σ (95% confidence limits) calendar age ranges in B.C. or A.D. calibrated with the CALIB 5.0.1 program [*Stuiver and Reimer*, 1993]. The

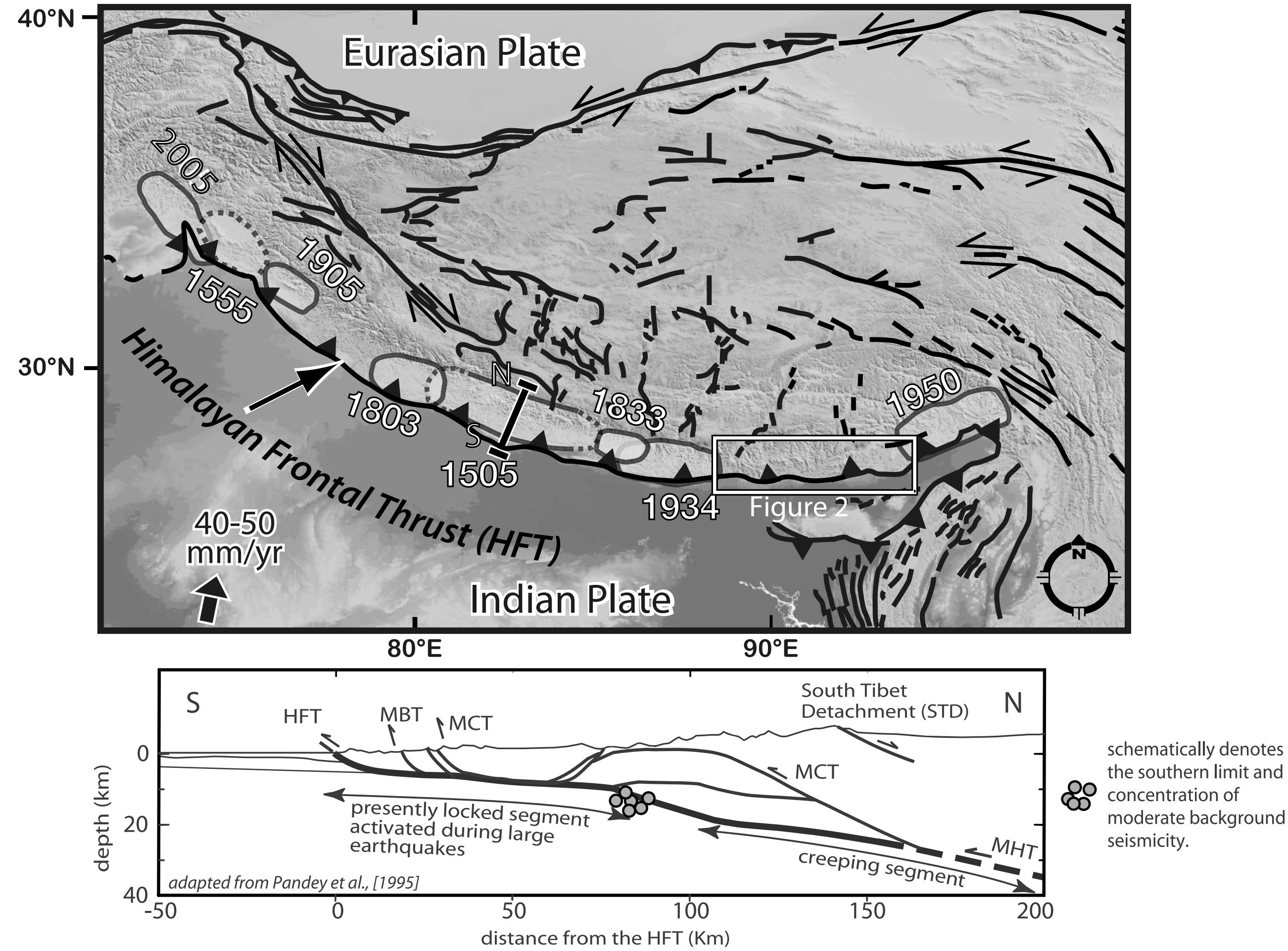

Figure 1. (top) Simplified map of distribution of active faults in northern India, Nepal, and Tibet [adapted from *Avouac and Tapponnier*, 1993; *Hussain et al.*, 2008]. The Himalayan Frontal Thrust (HFT) and inferred rupture extent (shaded and labeled with year) of major historical earthquakes along the ~2500 km Himalayan arc are shown. Dotted rupture extents are speculative. The rupture extent of the 1505 central Himalayan earthquake (M_w ~8.2), the 1555 Kashmir earthquake (M_w ~7.6), the 1803 Kumaon-Garhwal earthquake (M_w ~7.5), the 1833 Nepal earthquake (M_w ~7.3), the 1905 Kangra earthquake (M_w ~7.8), the 1934 Bihar-Nepal earthquake (M_w ~8.1), the 1950 Assam earthquake (M_w ~ 8.4), and the 2005 Kashmir earthquake (M_w 7.6) are adapted from published literature [*Ambraseys and Bilham*, 2000; *Ambraseys and Jackson*, 2003; *Ambraseys and Douglas*, 2004; *Bilham*, 1995; *Bilham*, 2004; *Bilham and Ambraseys*, 2005; *Chander*, 1989; *Martin and Szeliga*, 2010; *Molnar and Pandey*, 1989; *Pandey and Molnar*, 1988; *Szeliga et al.*, 2010; *Wallace et al.*, 2005] The extent of the map area shown in Figure 2 is outlined by white rectangular box. (bottom) Generalized North-south tectonic cross-section across the Himalaya. Location of section is indicated on map by a bold line with bars at end. Major thrust faults, the Main Central Thrust (MCT), the Main Boundary Thrust (MBT), and the HFT [*Gansser*, 1964; *Le Fort*, 1975; *Nakata*, 1972, 1989; *Yeats et al.*, 1992] sole into a major crustal décollement, the Main Himalayan Thrust (MHT). The cluster of small shaded dots schematically denotes the southern limit and concentration of moderate background seismicity [*Nelson*, 1998; *Pandey et al.*, 1995; *Schelling and Arita*, 1991; *Seeber and Armbruster*, 1981; *Zhao et al.*, 1993].

results, methodology, and laboratory used for radiocarbon analysis are summarized in Tables 1–3.

3. Site Descriptions, Trench Exposures, and Paleoearthquake Interpretations

[6] The HFT extends in the E-W direction for a length of ~2500 km from Pakistan in the west to Assam in northeast India (Figure 1). The geomorphic expression of the active HFT trace within the study area bounded between 88°E and 94°E is sinuous and discontinuous (Figure 2) and is manifested by uplifted and truncated alluvial fans and river terraces. In this section, we first provide for context the geomorphic and geometrical expression of faulting at and near each of the trench sites. The stratigraphic and structural relations observed in the trench exposures across the fault are then presented and interpreted to place bounds on the

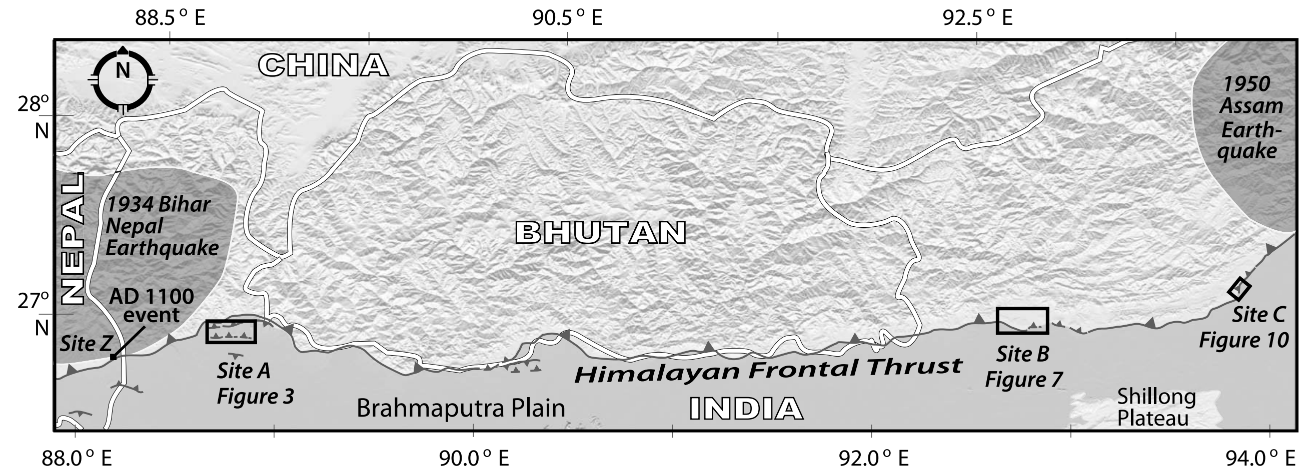

Figure 2. Ninety meter Shuttle Radar Topographic Mission (SRTM) map of the northeastern portion of the Himalaya (outlined by white rectangular box in Figure 1) showing location of the HFT along strike of three sites of study discussed in this paper. International borders are shown as white bold lines. Dark shaded polygons are the meizoseismal area of the 1934 Bihar-Nepal earthquake and the 1950 Assam earthquake [*Ambraseys and Douglas*, 2004; *Pandey and Molnar*, 1988]. The study sites, Chalsa (site A), Nameri (site B), and Harmutty (site C) are between the meizoseismal regions of the 1934 Bihar-Nepal and the 1950 Assam earthquake. Small boxes outline the approximate area of the HFT investigated for the present study. Active fault traces are adapted and modified after *Acharyya et al.* [1986], *Gansser* [1983] *Nakata* [1972, 1989], *Valdiya* [1992], and *Yeats et al.* [1992]. The A.D. 1100 event interpreted from a trench exposure by *Nakata et al.* [1998] and *Upreti et al.* [2000] in Nepal produced surface rupture, whereas the 1934 event apparently did not.

timing and size of the last surface-rupturing earthquake at each site.

3.1. Chalsa (Site A)

3.1.1. Chalsa Site Description

[7] Site A is located near the eastern border of Nepal (Figure 2). Geomorphic and neotectonic characteristics of faulting along the range and outboard of the range front near site A have previously been discussed in detail by *Nakata* [1972, 1989]. The site is situated in an embayment on the southernmost part of two HFT strands that strikes E-W for a distance of about ~30 km across the map area (Figure 3). River terraces (Qt1 and Qt2) and alluvial fan surface (Qaf1) offset by the HFT are preserved along the rivers Murti, Neora, and Jaldhaka [*Nakata*, 1972]. Two radiocarbon samples (Figure 3, site T2; Table 1, samples T2-E and T2-A) collected along the Neora River from a sand layer at the top of the Qt1 surface but below the zone of active soil formation yielded ages that range between calendar years (cal years) B.C. 1497 and 1311, or about 3500 years old. The surface and samples are situated about 21 m above current stream grade. All terraces and alluvial fan surfaces are truncated by the east trending HFT. As originally noted by *Nakata* [1972], the HFT in this area is delineated by prominent south facing scarps. The northernmost strand near the village of Matiali displaces alluvial fan and terrace surfaces (Qaf1, Qaf2, Qt1, and Qt2) to form scarps that stand 50 m across Qaf1 and 15 m across Qt1 (Figure 3). The western limit of the northern fault trace in the Qt1 terrace surface and the Qaf1 alluvial fan surface is very diffuse and not well defined. Along the southern trace to the north of the towns Dam Dim and Mal, the fault trace is broad and diffuse, reaching a maximum height of ~60 m across the Qaf1 surface. To the east, near the town of Chalsa, scarps in the older alluvial fan (Qaf1) are more pronounced and steep, reaching a height of ~70 m. The trench was excavated across a 15 m high scarp along the southern trace of the HFT near the eastern termination of Qt1 terrace surface at N26.88 and E88.87. The location of the trench (~48 m long and up to 7.5 m deep) near the village of Chalsa is shown in both Figures 3 and 4. A ~600 m long profile constructed across the fault scarp near and parallel to the trench site shows a steep and abrupt scarp near the ~300 m mark (Figure 4) and broader inflection on the hanging wall closer to the ~200 m mark.

3.1.2. Trench Stratigraphy, Structure, and Paleoearthquake Interpretation

[8] A log of the trench exposure is shown in Figures 5 and 6. The exposure is divided into three units on the basis of grain size, texture, color, and inferred depositional environment. Units 1 through 3, from bottom to top, in the hanging wall and footwall are correlative and bear the same label in Figures 5 and 6. Unit 1 consists primarily of poorly sorted, rounded to subrounded, cobble-boulder fluvial gravels. The upper portion of the unit is further distinguished by a clean white, poorly sorted, sand matrix. The lighter color is due to leaching associated with soil-forming processes. The dip of the unit approaches horizontal at the northern end of the trench. Intermediate unit 2 is predominantly pebble-cobble gravel in a sandy matrix overprinted by oxidation and local concentration of manganese oxide. Unit 2 is distinguished from the underlying unit 1 by a generally lesser clast size and greater degree of orange coloration due to oxidation. The uppermost and youngest sediments on the hanging wall (unit 3) consist of a black organic rich clayey silt to fine sand, with occasional pebbles

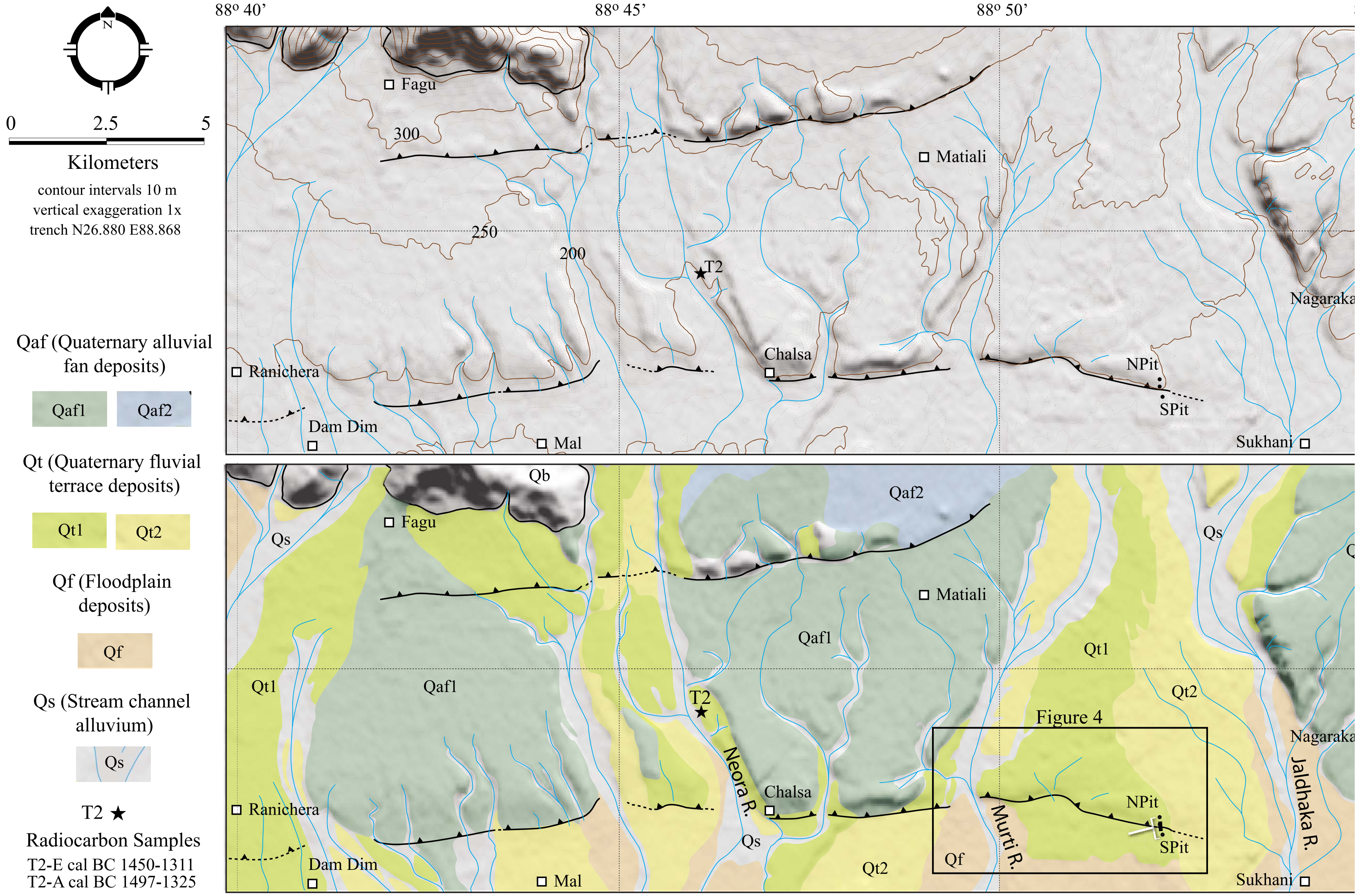

Figure 3. (top) Digital topography and major tectonic features of the Chalsa trench site in West Bengal (Figure 2, site A). Topography is from 90 m SRTM data (http://glcf.umiacs.umd.edu/data/srtm/). Contours are at 10 m intervals. (bottom) Quaternary geologic map of the study area showing the distribution of alluvial fan and terrace deposits along the Neora, Murti, and Jaldhaka Rivers. Map is modified and adapted after *Nakata* [1972]. The trace of the HFT where distinct is shown as solid line with teeth on the hanging wall and as a broken line where inferred. Location of radiocarbon samples obtained from a pit on top of the Qt1 surface is shown as a solid star (T2). Trench location and outline of Figure 4 are also labeled and shown. Coordinates of trench taken with handheld Garmin eTrex Vista GPS.

Table 1. Chalsa Calibrated ^{14}C Age[a]

CAMS Lab Code	Sample ID[b]	Unit ID	Uncalibrated Conventional ^{14}C Age (68% (1σ) cal age, in cal years B.P.)[c,d]	∂^{13}C Reported[e]	F^{14}C[f]	∂^{13}C Corrected ^{14}C Age (years B.P.)	95.4% (2σ) cal age (cal years A.D./B.C.)[a]	Relative Area Under Distribution
				Trench Samples				
134750	C 1	Unit 3	2445 + 35	−24.79	0.7376	2445 ± 35	B.C. 753–685	0.240
							B.C. 668–611	0.132
							B.C. 597–408	0.628
133588	C 2	Unit 3	3645 ± 30	−25.99	0.6350	3645 ± 30	B.C. 2134–2078	0.226
							B.C. 2071–2071	0.001
							B.C. 2063–1936	0.767
							B.C. 1933–1929	0.004
134751	C 3	Unit 3	6505 ± 40	−26.84	0.4450	6505 ± 40	B.C. 5529–5546	0.709
							B.C. 5448–5378	0.291
134752	C 4	Unit 3	1905 ± 30	−27.07	0.7887	1905 ± 30	A.D. 25–43	0.042
							A.D. 46–175	0.927
							A.D. 192–211	0.031
134753	C 5	Unit 3	545 ± 30	−27.25	0.9345	546 ± 30	A.D. 1314–1356	0.372
							A.D. 1388–1435	0.628
133376	C 6	Unit 3	5805 + 35	−25.73	0.4853	5805 ± 35	B.C. 4767–4755	0.014
							B.C. 4728–4547	0.986
134754	C 7	Unit 3	840 + 30	−24.59	.9009	840 ± 30	A.D. 1058–1064	0.006
							A.D. 1068–1071	0.005
							A.D. 1155–1265	0.989
133377	C 8	Unit 3	1465 ± 35	−25.85	0.8333	1465 ± 35	A.D. 544–648	1.
133378	C 9	Unit 3	3055 ± 30	−26.75	0.6839	3055 ± 30	B.C. 1410–1260	0.989
							B.C. 1228–1221	0.011
133587	C-A	Unit 3	5605 ± 30	−25.18	0.4976	5605 ± 30	B.C. 4493–4360	1.
133589	C-B	Unit 3	3375 ± 30	−25.03	0.6570	3375 ± 30	B.C. 1747–1607	0.981
							B.C. 1571–1560	0.012
							B.C. 1547–1540	0.007
134755	C-C	Unit 3	3410 ± 30	−4.94	0.6542	3410 ± 30	B.C. 1866–1849	0.027
							B.C. 1773–1624	0.973
134756	C-D	Unit 3	5710 ± 30	−25.86	0.4912	5710 ± 30	B.C. 4677–4675	0.003
							B.C. 4669–4660	0.012
							B.C. 4654–4639	0.026
							B.C. 4618–4460	0.959
134757	C-E	Unit 3	2395 ± 30	−27.18	0.7423	2395 ± 30	B.C. 728–692	0.070
							B.C. 658–654	0.005
							B.C. 542–396	0.925
134758	C-F	Unit 3	3045 ± 30	−24.87	0.6845	3045 ± 30	B.C. 1407–1256	0.924
							B.C. 1237–1215	0.046
133586	C-G	Unit 3	5055 ± 30	−23.49	0.5331	5055 ± 30	B.C. 3953–3783	1.
				Terrace Samples				
133379	T2 A	Terrace	3150 ± 30	−27.69	0.6756	3150 ± 30	B.C. 1497–1384	0.986
							B.C. 1332–1325	0.014
133380	T2 E	Terrace	3115 ± 30	−25.78	0.6784	3117 ± 30	B.C. 1498–1386	1.

[a]Calibrations were performed with Calib 5.0.1 (available at http://calib.qub.ac.uk/calib/) [*Stuiver and Reimer*, 1993]. Calibration data set: intcal04.14c [*Reimer et al.*, 2004]. Calibration curve: 2 (Northern Hemisphere terrestrial sample).

[b]Samples IDs have had a CO_2 split taken for ∂^{13}C analyses.

[c]Cal age = calendar age; cal year = calendar year.

[d]The quoted age is in radiocarbon years using the Libby half-life of 5568 years and following the conventions of *Stuiver and Polach* [1977].

[e]∂^{13}C values are the assumed values according to *Stuiver and Polach* [1977] when given without decimal places. Values measured for the material itself are given with a single decimal place.

[f]F^{14}C = A_{SN}/A_{ON} in notation of *Stuiver and Polach* [1977].

and cobbles. It is the organic-rich component of the capping soil.

[9] The subhorizontally dipping hanging wall units 1 through 3 gradually increase in dip toward the south and bend abruptly downward to form a ramp (or dip panel) that parallels the surface expression of the scarp. Units 1 and 2 in the hanging wall are truncated by a very shallow north dipping (~2°N–5°N) basal thrust fault marked F1 in Figures 5 and 6. The base of unit 1 is folded, overturned, and hence thickened at its southern limit on the hanging wall. Unit 2 is also overturned and thickened at its southern termination in the hanging wall. The overturning and thickening are interpreted to be the result of folding due to drag along the fault during displacement. The chaotic texture within the southern limit of unit 2 on the hanging wall above the fault may also reflect the collection and bulldozing of material along the fault front during displacement and a colluvial component dating to shortly after the most recent displacement. Unit 3, the organic-rich component of the soil, extends across the entirety of the exposure and is faulted and overridden by the fault F1. A very thin veneer of colluvium localized near the fault tip and further soil development have mantled the surface since the fault displacement.

Table 2. Nameri Calibrated ^{14}C Age[a]

CAMS Lab Code	Sample ID	Unit ID	Uncalibrated Conventional ^{14}C Age (68% (1σ) cal age, in cal years B.P.)[b,c]	∂^{13}C Reported[d]	F^{14}C[e]	∂^{13}C Corrected ^{14}C Age	95.4% (2σ) cal age (cal years A.D./B.C.)[a]	Relative Area Under Distribution
136945	N2[f]	Unit 5	1250 ± 35	−27.90	0.8586	1225 ± 30	A.D. 690–750	0.266
							A.D. 762–885	0.734
139837	N5	Unit 5	7145 ± 50	−25	0.4108		B.C. 6099–5693	0.872
							B.C. 5690–5899	0.128
139838	N6	Unit 5	1405 ± 35	−25	0.8395		A.D. 581–670	1.
136946	N7	Unit 9	1840 ± 35	−25	0.7951	1840 ± 35	A.D. 81–246	1.
139839	N8	Unit 5	935 ± 30	−25	0.8899		A.D. 1025–1163	1.
139840	N9	Unit 5	2210 ± 35	−25	0.7596		B.C. 383–196	1.
136947	N10[f]	Unit 9	1405 ± 40	−24.26	0.8390	1410 ± 35	A.D. 578–667	1.
139841	N12	Unit 5	925 ± 35	−25	0.8910		A.D. 1025–1185	0.994
							A.D. 1203–1205	0.006
139843	N19	Unit 5	1220 ± 35	−25	0.8591		A.D. 688–753	0.242
							A.D. 760–889	0.758
136948	N20[f]	Unit 5	1040 ± 35	−27.86	0.8809	1020 ± 30	A.D. 903–914	0.108
							A.D. 969–1045	0.896
							A.D. 1095–1120	0.042
							A.D. 1141–1147	0.009
136949	N21	Unit 9	1540 ± 30	−25.82	0.8258	1540 ± 30	A.D. 430–590	1.
136950	N22[f]	Unit 5	895 ± 35	−27.45	0.8967	875 ± 30	A.D. 1040–1110	.270
							A.D. 1116–1225	0.716
							A.D. 1234–1240	0.010
							A.D. 1248–1251	0.004

[a]Calibrations were performed with Calib 5.0.1 (available at http://calib.qub.ac.uk/calib/) [*Stuiver and Reimer*, 1993]. Calibration data set: intcal04.14c [*Reimer et al.*, 2004]. Calibration curve: 2 (Northern Hemisphere terrestrial sample).
[b]Cal age = calendar age; cal year = calendar year.
[c]The quoted age is in radiocarbon years using the Libby half-life of 5568 years and following the conventions of *Stuiver and Polach* [1977].
[d]∂^{13}C values are the assumed values according to *Stuiver and Polach* [1977] when given without decimal places. Values measured for the material itself are given with a single decimal place.
[e]F^{14}C = A_{SN}/A_{ON} in notation of *Stuiver and Polach* [1977].
[f]Samples IDs have had a CO_2 split taken for ∂^{13}C analyses.

Table 3. Harmutty Calibrated ^{14}C Age[a]

CAMS Lab Code	Sample ID	Unit ID	Uncalibrated Conventional ^{14}C Age (68% (1σ) cal age, in cal years B.P.)[b,c]	∂^{13}C Reported[d]	F^{14}C[e]	∂^{13}C Corrected ^{14}C Age	95.4% (2σ) cal age (cal years A.D./B.C.)[a]	Relative Area Under Distribution
136940	H7S[f]	Unit 1 FW	2210 ± 35	−26.77	0.7607	2195 ± 30	B.C. 367–181	1.
136940	H7S[f]	Unit 1 FW	2210 ± 35	−26.77	0.7607	2195 ± 30	B.C. 367–181	1.
136941	H10S[f]	Unit 1 FW	2045 ± 40	−26.91	0.7766	2030 ± 40	B.C. 164–129	0.079
							B.C. 120–A.D. 57	0.921
136942	H13S	Unit 1 HW	670 ± 35	−25	0.9203		A.D. 1272–1323	0.546
							A.D. 1346–1393	0.454
136943	H14S[f]	Unit 1 HW	715 ± 35	−26.13	0.9159	705 ± 30	A.D. 1259–1307	0.848
							A.D. 1362–1386	0.152
136944	H17S[f]	Unit 1 HW	695 ± 35	−25.71	0.9180	690 ± 30	A.D. 1266–1312	0.716
							A.D. 1358–1387	0.284
138647	H6S[f]	Unit 1 HW	855 ± 30	−25	0.8989		A.D. 1051–1081	0.079
							A.D. 1126–1135	0.015
							A.D. 1152–1259	0.906
138648	H9S[f]	Unit 1 HW	720 ± 30	−25	0.9145		A.D. 1228–1232	0.008
							A.D. 1238–1301	0.942
							A.D. 1367–1382	0.051
138649	H12S[f]	Unit 1 HW	1070 ± 30	−25	0.8755		A.D. 895–925	0.220
							A.D. 936–1021	0.780
138650	H15S	Unit 1 HW	1045 ± 30	−25	0.8778		A.D. 898–919	0.089
							A.D. 947–1029	0.911

[a]Calibrations were performed with Calib 5.0.1 (available at http://calib.qub.ac.uk/calib/) [*Stuiver and Reimer*, 1993]. Calibration data set: intcal04.14c [*Reimer et al.*, 2004]. Calibration curve: 2 (Northern Hemisphere terrestrial sample).
[b]Cal age = calendar age; cal year = calendar year.
[c]The quoted age is in radiocarbon years using the Libby half-life of 5568 years and following the conventions of *Stuiver and Polach* [1977].
[d]∂^{13}C values are the assumed values according to *Stuiver and Polach* [1977] when given without decimal places. Values measured for the material itself are given with a single decimal place.
[e]F^{14}C = A_{SN}/A_{ON} in notation of *Stuiver and Polach* [1977].
[f]Samples IDs have had a CO_2 split taken for ∂^{13}C analyses.

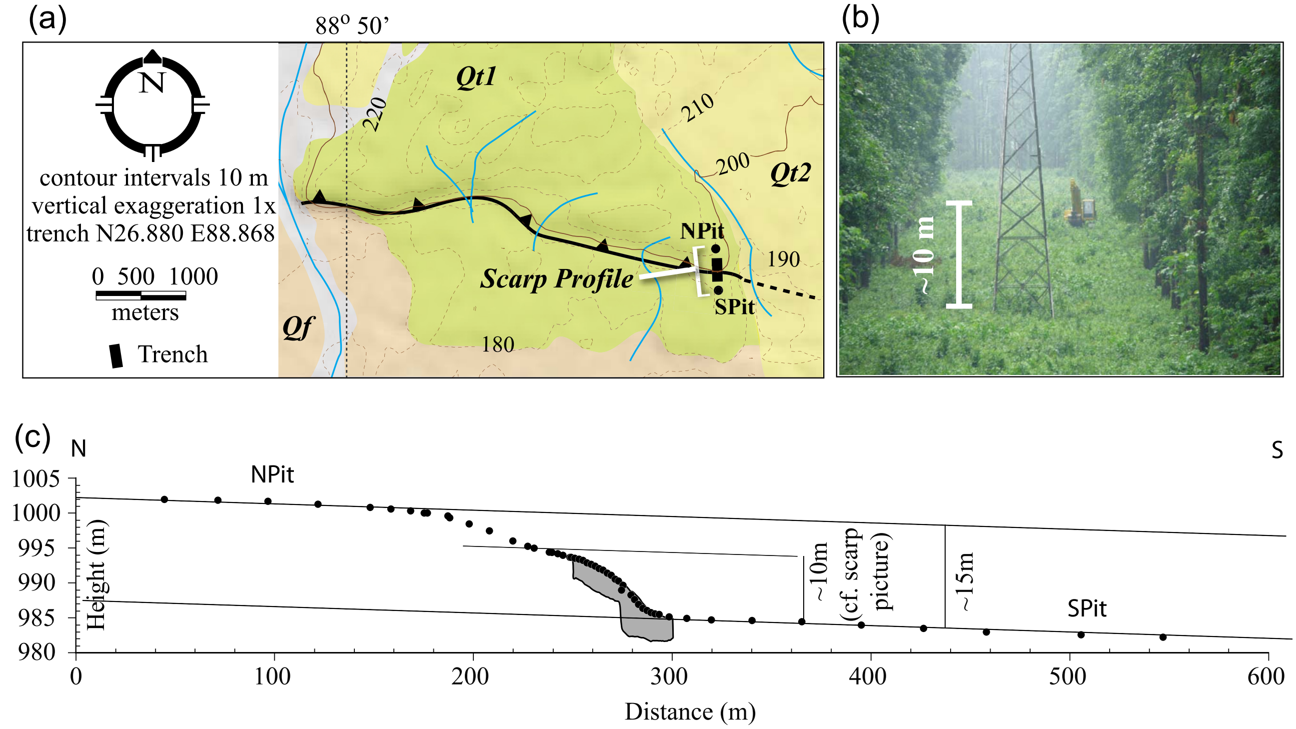

Figure 4. (a) Topographic map and profile of Chalsa site (Figure 2, site A). Location of trench (solid rectangle oriented north south), pits (solid circle), and profile (with line) are shown. (b) Photograph of the trench site, with track-hoe on the crest of the scarp for scale. Picture was taken from south looking towards north. (c) Profile across the fault scarp. (Vertical exaggeration = ~4.5×.) The profile was surveyed using an electronic distance measurement (EDM)/total station and shows an inflection on the hanging wall near the 230 m mark. The inflection may be the result of an older event or, equally plausibly, another strand of the fault that ruptured simultaneously with that observed in the trench. Coordinates of trench obtained with handheld Garmin Vista eTrex GPS.

3.1.3. Timing of the Earthquake

[10] The radiometric ages of 16 detrital charcoal samples taken from unit 3 places a limit on the timing of the surface rupture displacement (Figures 5 and 6; Table 1). The ages of the 16 samples collected from unit 3 show a wide variation of sample ages within the bed (Figure 6 and Table 1). Of the samples clearly underlying the fault, thus in the portion of unit 3 cut by the fault, the age ranges vary from cal years A.D. 544–648 (sample C-8) to cal years B.C. 4788–4544 (sample C-6). There is no clear spatial or stratigraphic relation of the age determinations to the respective locations of the samples along the span of the fault within unit 3, which we interpret as indicating the presence of reworked detrital charcoal within unit 3. From this, we interpret that the last surface displacement occurred after the period A.D. 544–648 (sample C-8). Yet younger ages are recorded by samples C-7 (cal years A.D. 1059–1266) and C-5 (cal years A.D. 1315–1435) located outboard and south of the fault tip within unit 3. Interpretation of the two ages is problematic because the samples are from a soil of massive character and the structural relationship of the two samples to the fault F1 is not definitive. Sample C-7 is located directly adjacent to and at an elevation just below the F1 fault tip and can be reasonably interpreted to have been present at the time of faulting, thus allowing that the most recent displacement occurred subsequent to cal years A.D. 1059–1266. The sample C-5 is about 3 m south of the fault tip and in the middle lower portion of unit 3. One might suggest from the sample that the most recent displacement of F1 is subsequent to cal years A.D. 1315–1435, though its presence in a soil and its distance from the fault would permit the interpretation that it was emplaced subsequent to the most recent displacement of F1 as well.

[11] The presence of detrital charcoal ages in the trench exposure that are significantly older than the ~3500 year old samples taken at site T2 along the Neora River (Figure 3) suggests that (1) either the fan element of unit Qt1 in which the trench is emplaced is significantly older than the element from which the samples T2-A and T2-E (Figure 3, site T2; Table 1) were taken, or (2) that the fan element at the trench site has perhaps incorporated older detrital charcoal from adjacent surfaces Qaf1. The lesser soil development observed at the sample sites along the Neora River as compared to the trench site suggests the former of the two is most likely.

[12] The correlation of displaced units 1–3 on the footwall and hanging wall, the apparently small amount of erosion of the dip panel above the fault, and the small amount and young age of a single-episode, fault-derived colluvium suggest that the exposure records displacement from only a single earthquake. The minimum displacement across the fault, F1, revealed in the trench is ~14 m, the distance along the fault from the base of the trench to the fault tip exposed in the trench (Figures 5 and 6). The amount and the shallow

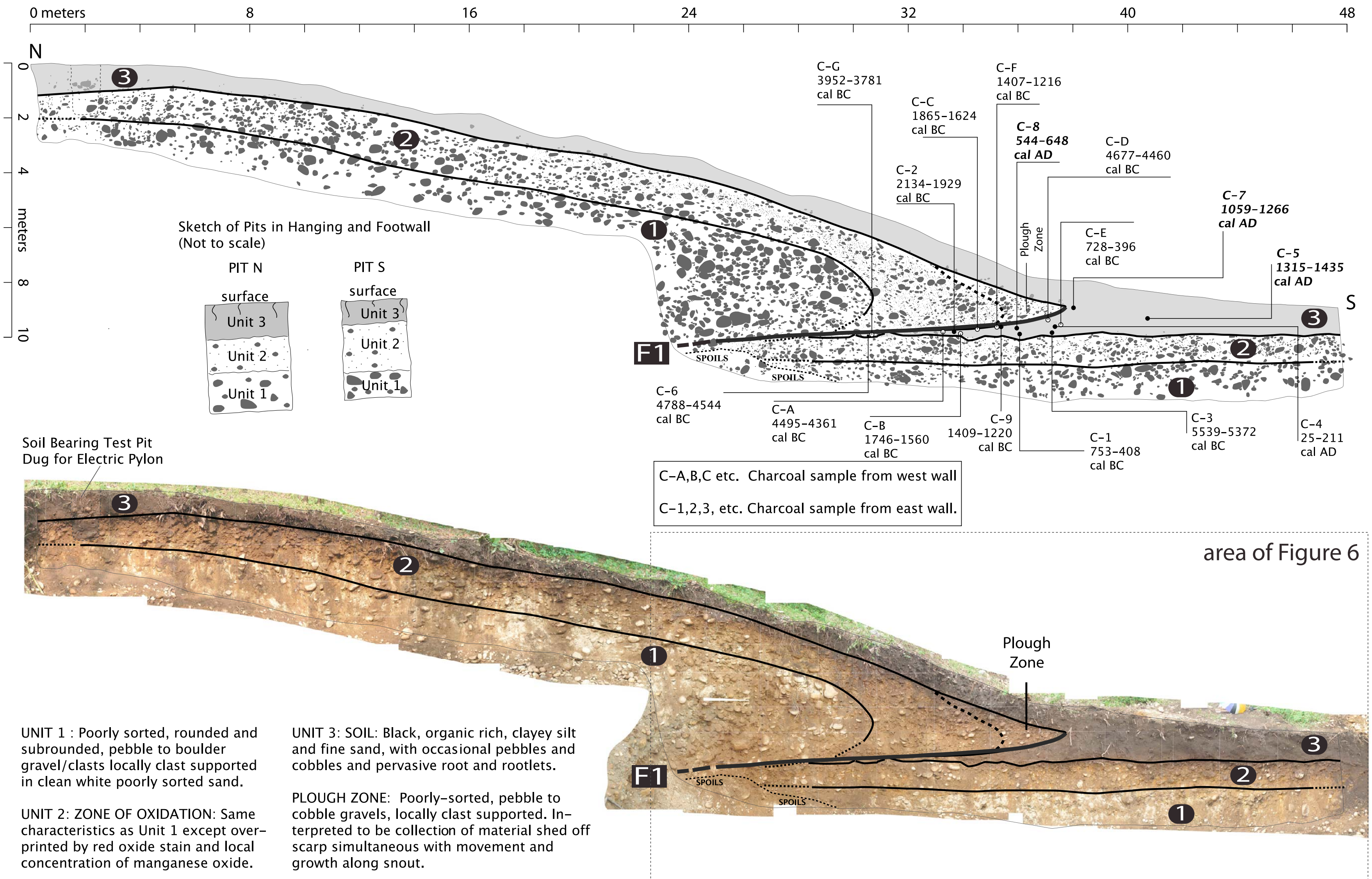

Figure 5. Illustrated and photographic log of east wall of Chalsa trench. Region outlined in box is further enlarged in Figure 6 to show details of crosscutting relationship and radiocarbon sample locations. Numbers in solid black circles denote the major stratigraphic units discussed in the text. F1 denotes principal fault strand exposed in the trench wall. Radiocarbon sample locations are denoted by black solid dots, and each is labeled to show sample number. Long bars and numbers in calendar year B.C. or A.D. that accompany each sample correspond to the ^{14}C age determinations of detrital charcoal (Table 1). Horizontal and vertical scales are in meters. No vertical exaggeration.

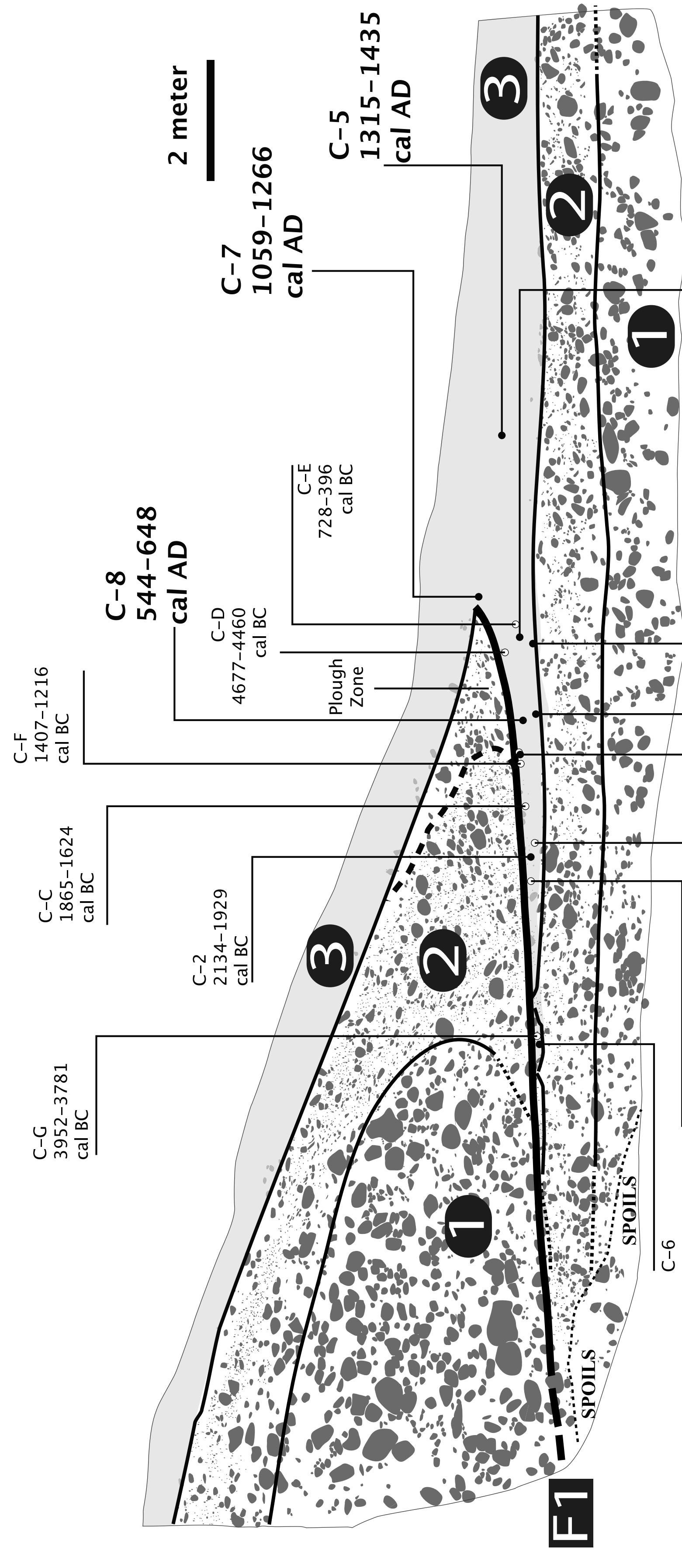

Figure 6. Portion of the Chalsa trench outlined by rectangular box in Figure 6. Detail shows structural relationship of radiocarbon samples and ages to the fault. Unit and fault labels are same as Figure 5. No vertical exaggeration.

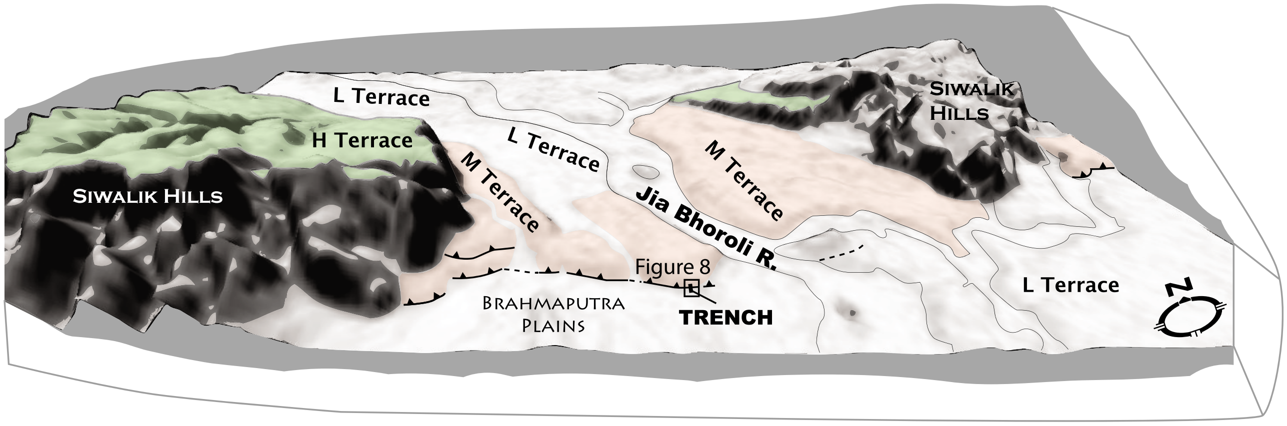

Figure 7. Distribution of fluvial terrace deposits and traces of the HFT (solid lines with teeth on hanging wall) near Nameri (Figure 2, site B) along the river Jia Bhoroli on a digital topographic map computed from 90 m SRTM data (http://glcf.umiacs.umd.edu/data/srtm/). Definition and relative ages of terraces based on the relative height from stream grade, soil development, and degree of dissection based on SRTM and field observation. Trench location and outline of Figure 8 are also shown.

dip of the fault on which displacement occurred is insufficient to explain the minimum ~10 m scarp produced by the displacement (see profile in Figure 4). The fault plane thus likely increases in dip to the north below the exposure and an additional component of fault offset is recorded in near-surface folding and tilting and in production of the dip panel that forms the scarp.

3.2. Nameri (Site B)

3.2.1. Nameri Site Description

[13] Site B is located east of site A between longitude 92.6°E and 92.8°E. (Figure 2). Faulting along the E-W trending HFT has uplifted fluvial sediments to produce broad abandoned Quaternary fluvial terrace surfaces along the Jia Bhoroli River (Figure 7). Progressively greater offsets on older fluvial terrace surfaces and decreasing offsets on younger fluvial terrace surfaces attest to recent and repeated fault displacement through the Quaternary at this site. Three distinct and broad fluvial terrace surfaces are mapped, in order of decreasing elevation: higher, middle, and lower terrace surfaces (Figure 7). The middle and lower terrace surfaces are most widely developed and preserved. Each is truncated by the HFT with the exception of the youngest lower terrace surface. The truncation of the higher and middle terrace surface by the HFT indicates that they have been abandoned and preserved primarily as a result of tectonic displacement along the underlying and north dipping HFT.

[14] The E-W trending HFT at its local eastern termination near the Jia Bhoroli River is expressed by a ~9 m high scarp (Figures 7 and 8). A picture of the scarp and trench site is shown in Figure 8. A topographic map of an area about 150 m × 800 m around the trench site and a profile of the scarp at the trench site are shown in Figure 8. The top of the surveyed middle terrace surface shows smooth undulatory topography and headwardly eroding streams. The scarp is markedly steeper along the lower 4 to 5 m of the scarp. The far-field slope of the footwall is subhorizontal to near horizontal while the hanging wall far-field slope is modified by a combination of agricultural practices and headwardly eroding stream channels.

3.2.2. Trench Stratigraphy, Structure, and Paleoearthquake History

[15] The 4.5 m depth of the ~20 m long trench was limited both by the small size of excavator available and a shallow water table (Figure 9). The trench stratigraphy exposed is subdivided into ten laterally continuous depositional units (units 1 through 10, oldest to youngest) of fluvial gravels, well-bedded sands, and silts (Figure 9). The oldest stratigraphic unit (unit 1) observed in the trench exposure is a fluvial gravel package composed of poorly sorted, well-rounded sand, cobble, and small boulder gravels. Portion of the unit 1, observed between the 8 and 12 m mark to the south, although, lacks clear expression of depositional fabric but is the same as unit 1 and suggests bulldozing of the material near the tip of the fault, F1. Unit 2 in the hanging wall overlies unit 1 and is characterized by massive fine sand with occasional pebble gravels. Overlying unit 3 is a silty-clay loam overbank deposit with incipient soil development. Unit 4, observed at the base of the trench in the footwall, is a dark yellowish brown, clean, fine to very fine sand with very fine planar interbeds of darker sandy-silty clay beds. Unit 5 is dark green silty sandy clay displaying numerous irregular small blobs of oxidation that give the unit a mottled appearance. Unit 6, which sits on top of unit 5, is a very thin layer of dark gray silty clay. Darkening due to soil development and numerous wormholes indicate that the unit was a paleosurface. Unit 7, observed near the northern part of the exposure between meter marks 2–7, is a wedge-shaped unit consisting of sheared brown to yellowish brown sandy clay. Unit 8 locally overlies units 1 and 6. The contact between unit 6 and overlying unit 8 near meters 12 to 14 is marked by a sharp and abrupt contact. Unit 8 consists of numerous interbedded and deformed fine grained to very fine grained sands and sandy-silty clays. The sand is predominantly grey in color with occasional red coloration due to oxidation. Fabric highlighted by oxidation shows folding and warping around the nose of unit 1. Unit 9 is similar in character to unit 4 and unit 8, and it consists of

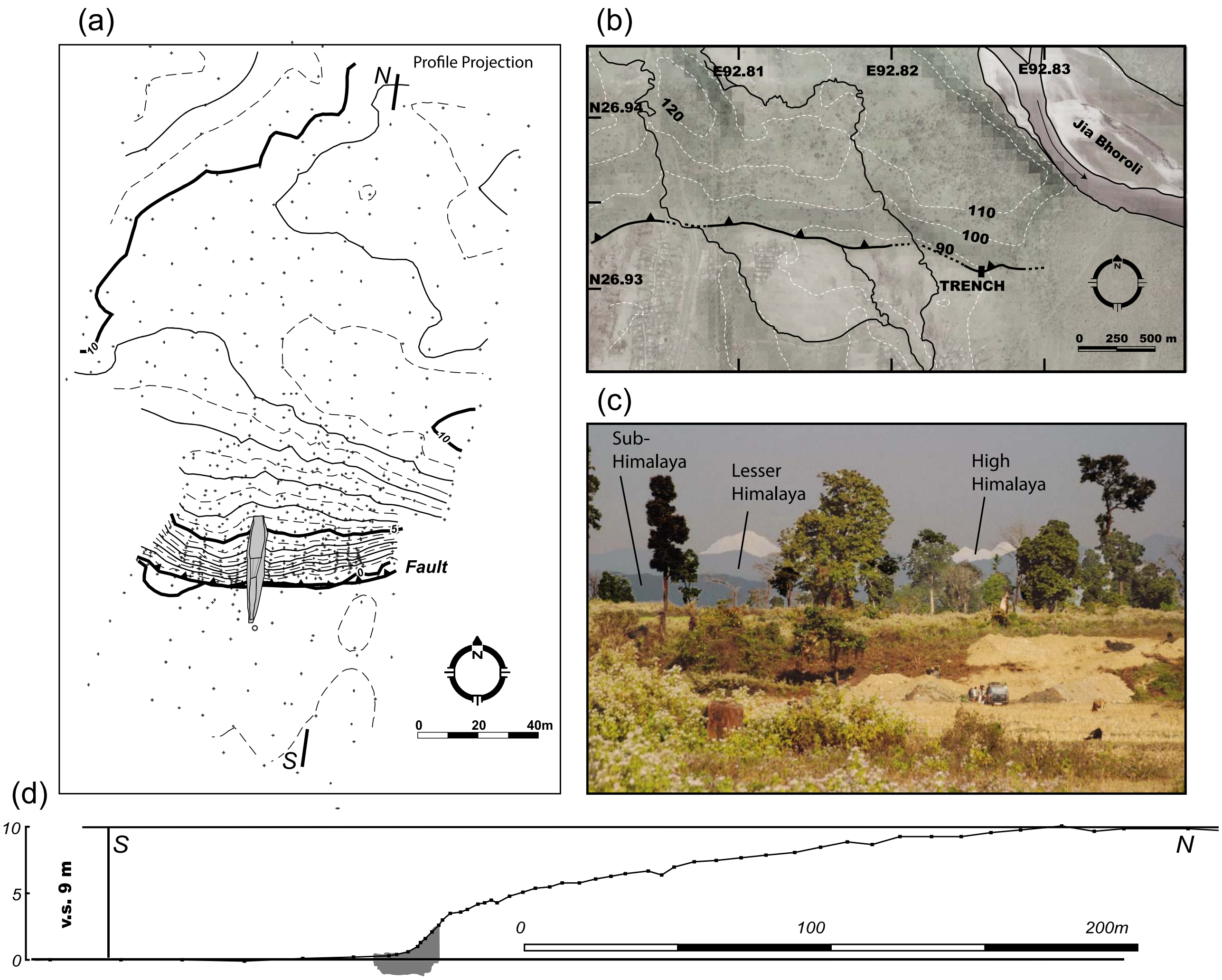

Figure 8. (a) Topographic map of Nameri site (Figure 2, site B) shows locations of trench (polygon oriented N-S) and location of the N-S topographic profile provided at bottom (4.5 × vertical exaggeration). Contours on topographic map are at 0.5 m intervals and are based on survey using a tripod and a Trupulse laser distance and angle measuring device. (b) A smaller-scale topographic map overlaid on a Google Earth image of the site is shown; (c) a ground photograph of the site (a backhoe on the crest of the scarp and jeep near the base of the scarp provide scale). Picture was taken from the south looking north. (d) North-south profile across the fault scarp and projection of the trench. Coordinates of trench obtained with handheld Garmin Vista eTrex GPS.

numerous planar interbedded and deformed fine to very fine sands and sandy-silty clays. The contact between units 8 and 9 is poorly defined or unclear. Unit 10 sits on top of units 8 and 9 and consists of poorly sorted, well-rounded pebble to small cobble gravels derived from unit 1.

[16] Basal units 4–6 are truncated and overlain by a fault (F1) in the northern portion of the trench (Figure 9). Likewise, hanging wall units 1–3 have been transported southward and upward along the relatively shallow dipping thrust plane. The fault (F1) is manifested as a relatively thick shear zone near the northern end of the trench (unit 7), where it dips downward at ~12° and is a discrete, essentially horizontal contact, to the south. The total distance of fault contact exposed in the trench is about 12 m.

[17] The fault apparently splits into two strands at meters 8 to 9 (Figure 9). The upward splay marks the basal contact of northern facies of unit 8. The similarity in color and texture of units 8 and 4 leads to the interpretation that they are the same units now displaced by the fault, requiring ~7 to 8 m of displacement. However, a villager's account indicates that location of unit 8 directly underlying unit 10 is an abandoned, hand-dug irrigation canal. This would suggest that units 8 and 10 may be infill, in which case the dipping laminae in unit 8 may be due to gradual fill of the canal rather than tectonic deformation and emplacement, and thus the underlying fault trace beneath unit 8 may be due to human disturbance. Accepting that it is a fault would lead to interpretation of at least ~7 to 8 m of displacement measured from the fault exposed near the base of the trench to the tip of the fault over unit 1. The lower of the two strands continues southward to about meter 14 and records greater offset. The greater offset is derived from the observations that (1) the texture and color of sediments of unit 9 around the nose of unit 1 are the same as units 4 and 5

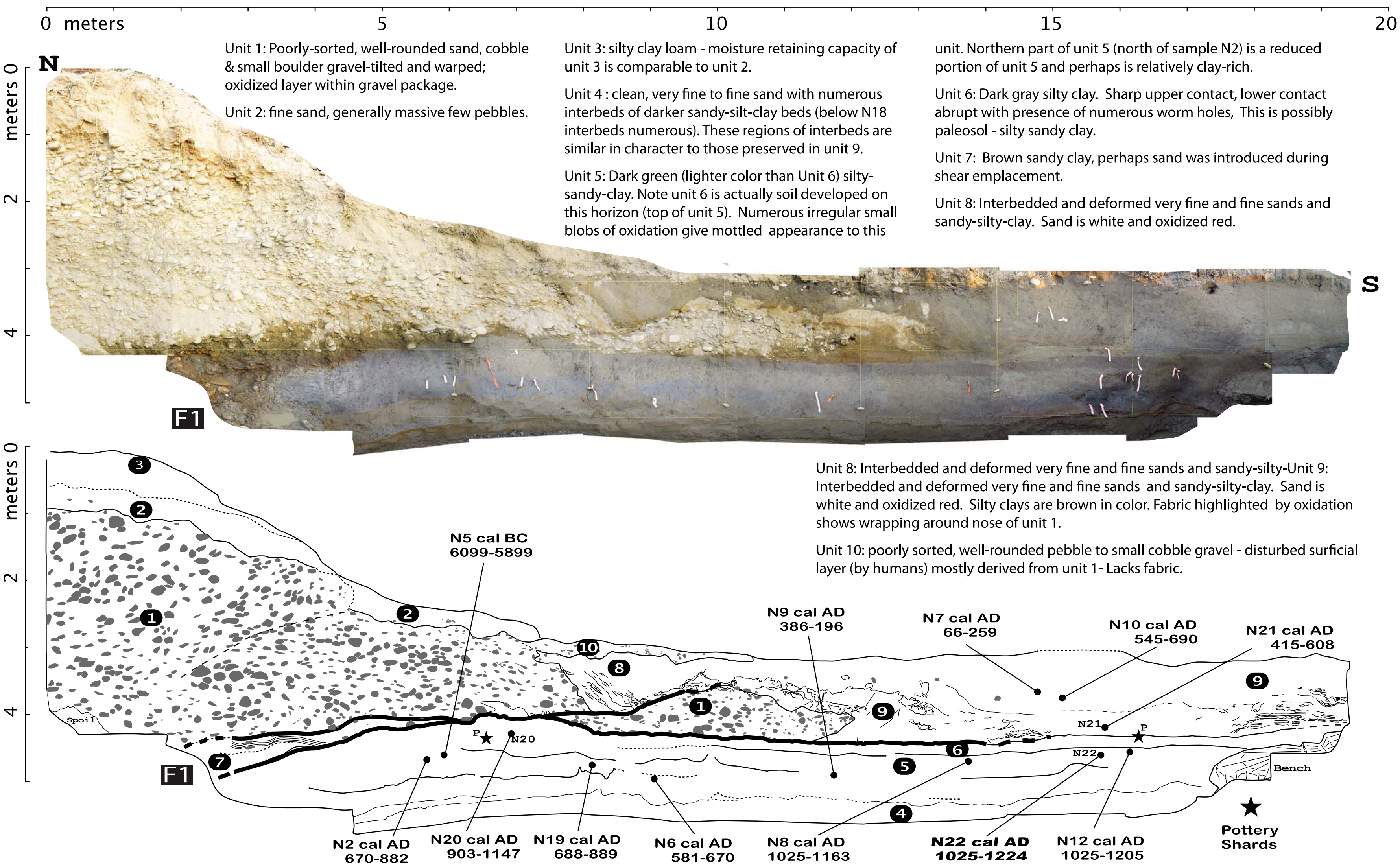

Figure 9. Log of the east wall of Nameri trench. Numbers in solid black circles denote the major stratigraphic units discussed in the text. Annotation "F1" denotes principal fault strand exposed in the trench wall. Radiocarbon sample locations and sample numbers of the detrital charcoal samples are shown as solid black dots. The solid black stars denote the location of pottery shards. Long bars and numbers in calendar year B.C. or A.D. that extend from each sample correspond to the ^{14}C age determinations of detrital charcoal (Table 2). Horizontal and vertical scales are in meters. No vertical exaggeration.

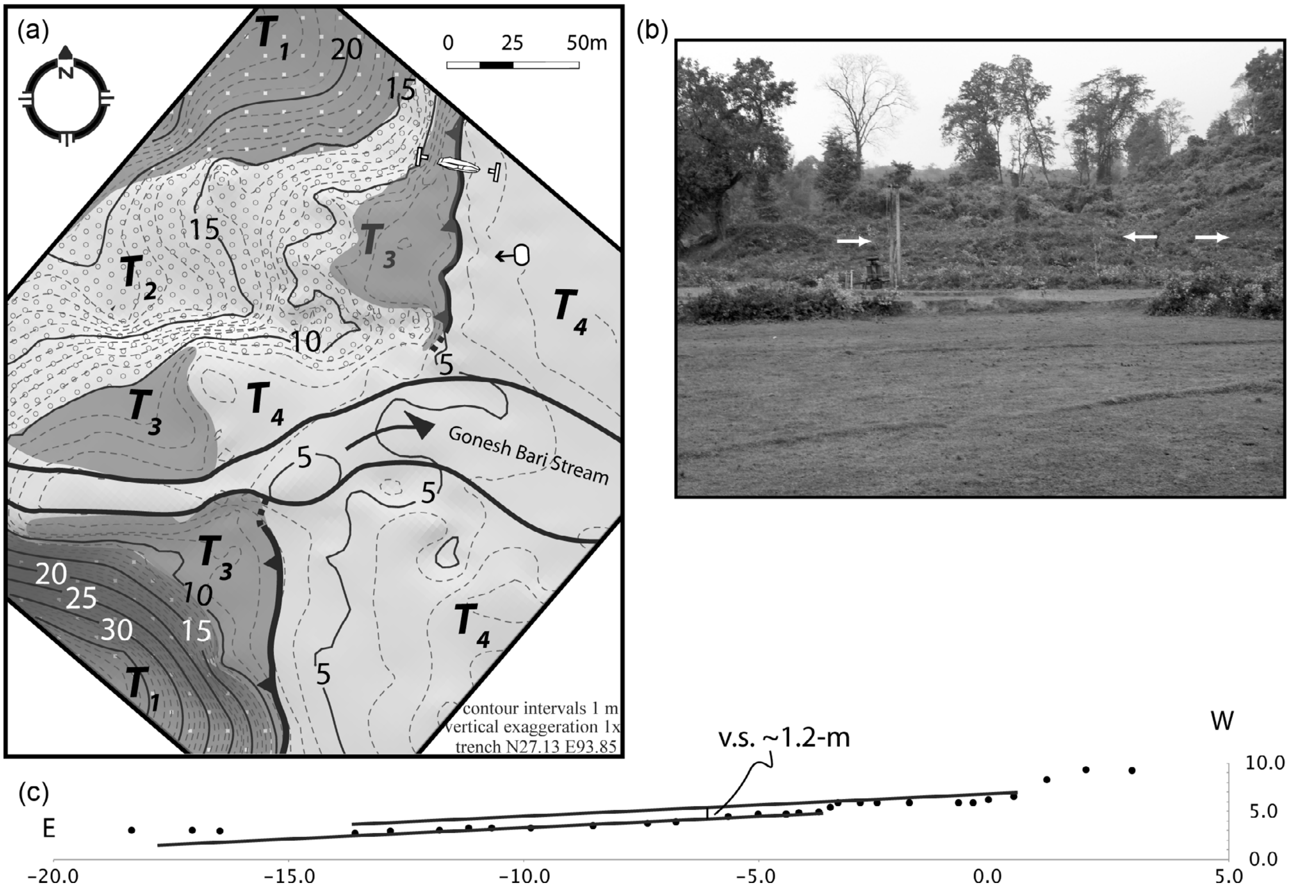

Figure 10. (a) Topographic map, location of trench (polygon oriented E-W) and E-W scarp profile at Harmutty Tea Estate (Figure 2, site C). Topography and field observations are used to label different levels of terrace surfaces preserved along Gonesh Bari Stream. Contours on topographic map are at 1 m intervals and are based on survey using a tripod and a Trupulse laser distance and angle measuring device. (b) Photograph of the trench site. Ellipse with arrow on topographic map at left points in the direction of photograph. White arrows are aligned parallel and along the crest of fault scarp across which trench was excavated to produce log shown in Figure 11. (c) E-W profile across the fault scarp (vertical exaggeration = 5×). Coordinates of trench obtained with handheld Garmin Vista eTrex GPS.

and (2) the ages of detrital charcoal collected from unit 9 are older than the ages of detrital charcoal taken from directly below the fault (F1) in units 5 and 6 (Figure 9). The similarity in color and texture and the presence of older ages above the fault with respect to those directly below are consistent with emplacement of unit 9 and the northern portion of unit 9 by thrust displacement. The southernmost exposure of unit 9 displays horizontal laminae and likely reflects growth stratigraphy after the last displacement. The observations interpreted in this manner point to a displacement of units 8 and 9 equal to a minimum displacement of 12 meters.

3.2.3. Timing of the Earthquake

[18] Radiocarbon ages of detrital charcoal samples are summarized in the trench log of Figure 9 and Table 2. The range of 7 sample ages in units 4 and 5 below the fault F1 range from cal years A.D. 581–670 (sample N6) to cal years A.D. 1025–1224 (sample N22), with the exception of the outlier of sample N5 that dates to cal years 6099–5899 B.C. The fault displacement most reasonably postdates the youngest of these values (sample N22, cal years A.D. 1025–1224). Samples N7, N10, and N21 taken from unit 9 that sit above the fault are older than the limiting age provided by sample N22 and provide no basis to assign an upper (more recent) bound on the age of the last earthquake displacement. They are more likely correlated to the ages of samples taken from units 5 and 6 and, as previously described, reflect tectonic emplacement.

3.3. Harmutty (Site C)

3.3.1. Harmutty Site Description

[19] Site C is located at longitude ~93.8°E, just west of the meizoseismal zone and within the region of strong shaking of the M_w ~ 8.4 1950 Assam earthquake (Figures 2 and 10). The strike of the HFT bends northward to a near N-S strike in the vicinity of the Harmutty trench site (Figure 2). Fault scarps in Quaternary alluvium are here evident along the main trace of the HFT where it cuts and uplifts fluvial terrace deposits of progressively increasing age, indicating repeated fault displacements through the Quaternary period (Figure 10). Figure 10 contains a topographic map, photo, and scarp profile at the trench site.

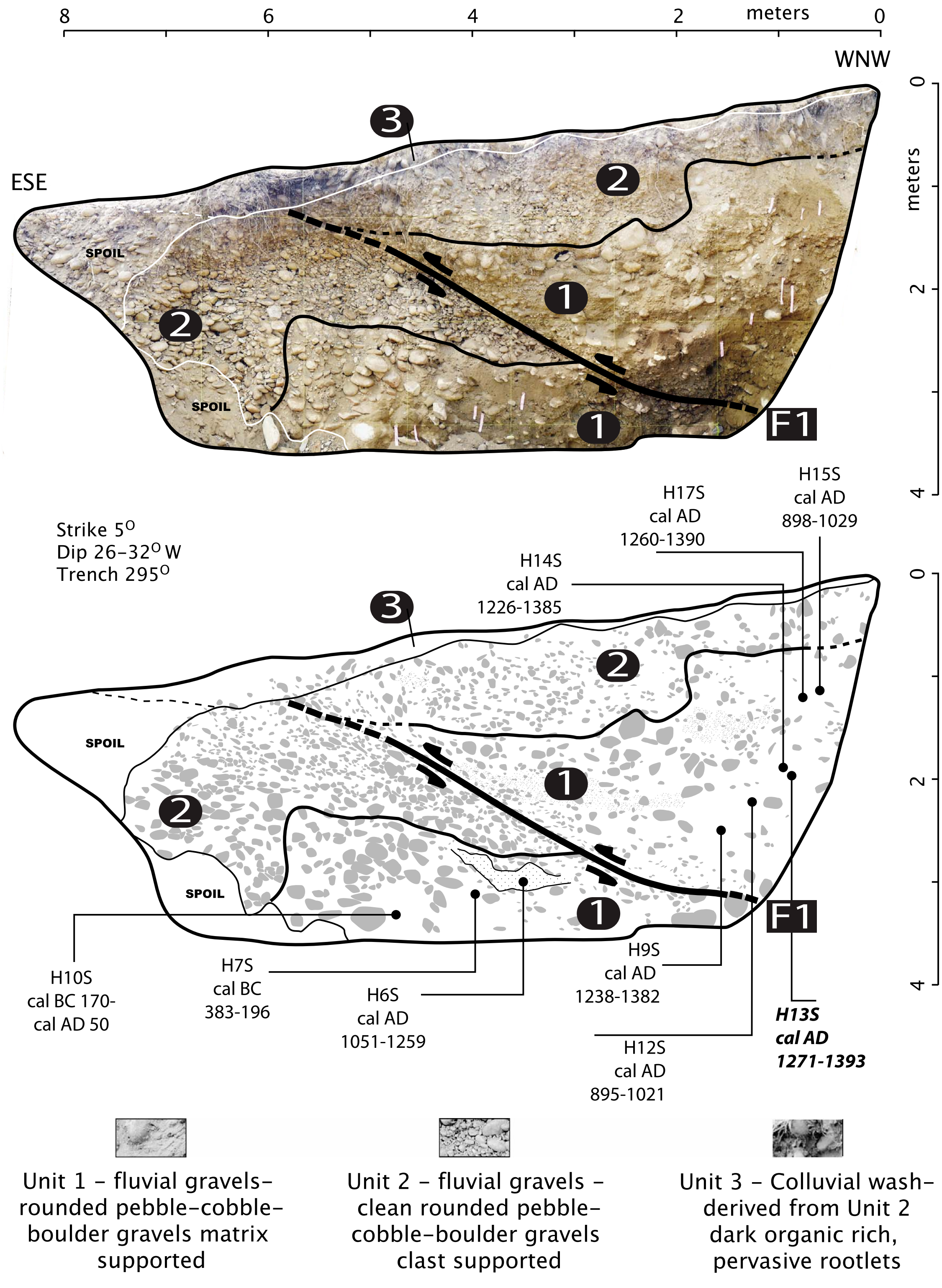

Figure 11. Log of south wall of Harmutty trench. Numbers in solid black circles denote the major stratigraphic units discussed in the text. Annotation "F1" in solid black square denotes principal fault strand exposed in the trench wall. Small solid dots and associated numbers show the location and sample number of the detrital charcoal samples, respectively (Table 3). Long bars and numbers in calendar year A.D. or B.C that extend from each sample correspond to the ^{14}C age determinations of detrital charcoal samples (Table 3). Horizontal scale is the distance along the trench in meters, as measured from the west end of the trench. Vertical scale is meters below arbitrary vertical datum near the top of the north end of the trench. No vertical exaggeration.

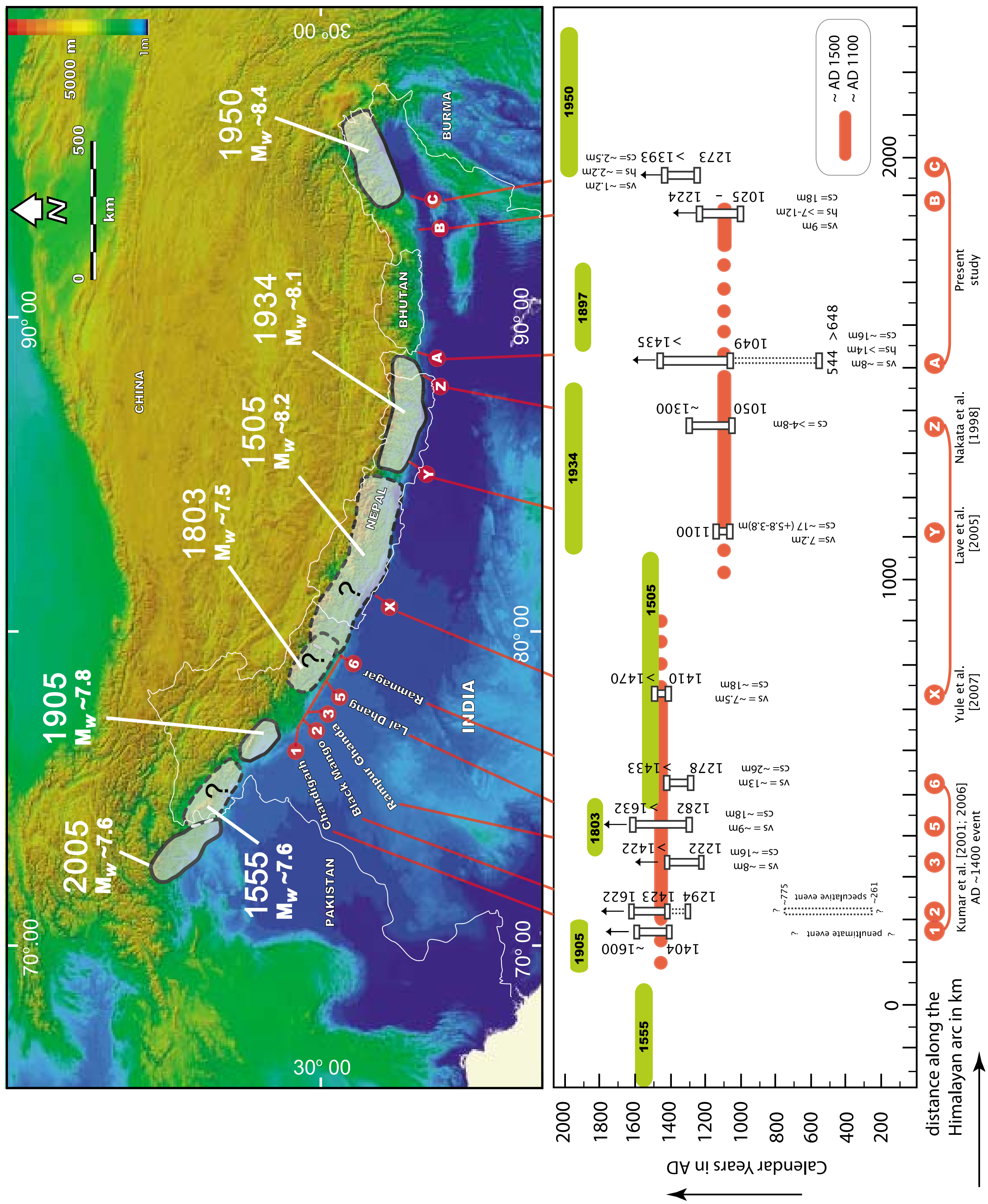

2005 Mw ~7.6
1555 Mw ~7.6
1905 Mw ~7.8
1803 Mw ~7.5
1505 Mw ~8.2
1934 Mw ~8.1
1950 Mw ~8.4
CHINA
PAKISTAN
INDIA
NEPAL
BHUTAN
BURMA
Chandigarh
Black Mango
Rampur Ghanda
Lal Dhang
Ramnagar
N
km
5000 m
1 m
Calendar Years in AD
distance along the Himalayan arc in km
~ AD 1500
~ AD 1100
Kumar et al. [2001; 2006] AD ~1400 event
Yule et al. [2007]
Lave et al. [2005]
Nakata et al. [1998]
Present study
penultimate event
speculative event

Figure 12

[20] At the trench site, three levels of well-developed, uplifted, and abandoned terrace surfaces are present along the Gonesh Bari Stream (Figure 10). The three terraces from oldest to youngest are labeled T1, T2, and T3. Each surface is cut and displaced by the roughly N-S trending HFT and thus bounded by an east facing fault scarp. The faulted T3 surface produces a vertical separation of ~1.2 m (Figure 10). Fluvial terrace surface T4 sits lower and is not cut by the fault, and the extension of the T4 surface merges downstream with the Gonesh Bari stream grade.

3.3.2. Trench Stratigraphy and Structure

[21] The trench exposed three distinct stratigraphic units. Each is labeled from oldest to youngest, respectively, as units 1, 2, and 3 (Figure 11). Unit 1, the oldest unit observed at the base of the trench, consists of predominantly poorly sorted rounded pebble-cobble-boulder fluvial gravels in a sandy matrix. Unit 2 overlies unit 1 along an irregular sharp contact. Unit 2 is a wedge-shaped, very loose, clast-supported, pebble-cobble, cut-and-fill channel deposit that is about 0.5 m in thickness near the western wall of the trench and thickens eastward gradually to about 1.5 m (Figure 11). Unit 3 is the youngest unit observed at the top of the trench and consists of slope-derived colluvial wash from units 1 and 2. Poorly sorted rounded pebble-cobble gravels capped by a thin veneer of modern root and organic-rich silty-sand deposits characterize unit 3. Unit 3 is thinnest near the western end of the trench wall and gradually thickens towards the east to about 30–40 cm.

[22] Units 1 and 2 are cut by the fault plane F1 (Figure 11). Displacement along the fault F1 has transported the western portions of the units 1 and 2 up and over the eastern portion of the exposed units. The fault F1 is a planar west-dipping (~26°W–32°W) fault characterized by a single narrow shear zone along most of its length (Figure 11). The thrust (F1) has transported the hanging wall units 1–2 onto the footwall units 1–2. Overlying unit 3 sits on top of the fault strand F1 and is not cut by the fault. Displacement along fault F1 extends from the base of the exposed trench up to the base of the stratigraphic level of unit 3. The displacement and associated scarp are interpreted to be the result of a single event displacement based on the presence of only a single thin colluvial wedge (unit 3) and a lack of buried scarps or other truncated fault strands within the exposed trench wall. A maximum slip of ~2.5 m is recorded in the trench exposure by thrusting of the contact between units 1 and 2. The amount of vertical separation in the trench measured from the base of unit 2 (Figure 11) and from the hanging and footwall of the long profile (Figure 10) is ~1.2 m.

3.3.3. Timing of the Earthquake

[23] Accelerator mass spectrometer radiocarbon (^{14}C) analyses of nine detrital charcoal samples collected from the Harmutty trench provide an age constraint on the timing of fault displacement recorded in the trench (Figure 11 and Table 3). All the samples are from the faulted oldest unit 1, and the detrital charcoal samples yielded a wide range of ages, ranging from cal year 383 B.C. to cal year A.D. 1393 (Table 3) that display no clear relationship to stratigraphic position within unit 1. The wide span of ages is interpreted to reflect the presence of reworked detrital charcoal. No samples were observed or collected in overlying unit 2. From these observations, we interpret that the displacement occurred subsequent to cal years A.D. 1271–1393 (sample H13S), the youngest of the ages of detrital charcoal collected from unit 1. The vertical separation of the ground surface across the scarp at the Harmutty trench is ~1.2 m (Figure 10), which is virtually the same as the vertical offset of the base of unit 2 or the top of unit 1 (Figure 11). The displacement is considerably smaller than that observed in the Chalsa and Nameri trenches.

4. Summary and Conclusions

[24] Prior paleoseismic studies have been distributed along the western two-thirds of the HFT, extending ~1500 km through northwest India and along the southern border of

Figure 12. Synopsis of historical and paleoseismic history along the HFT. (top) Digital topography is from 90 m SRTM data (http://glcf.umiacs.umd.edu/data/srtm/). Shaded areas with bold outline or dotted line in map view correspond to areas of strong ground shaking associated with historical earthquakes. Each is labeled with the corresponding age and magnitude of the earthquake. Solid circles with numbers and letters are location of trench studies described here for sites A through C in the northeast Himalaya, along with previously reported at sites 1–6 in the northwest Himalaya and sites X through Z in Nepal [*Kumar et al.*, 2001; *Kumar et al.*, 2006; *Lavé et al.*, 2005; *Nakata et al.*, 1998; *Upreti et al.*, 2000; *Yule et al.*, 2006]. (bottom) Space-time diagram showing radiocarbon constraints on timing of surface rupture earthquakes documented at each site. Vertical axis is time in calendar years A.D.; horizontal axis is kilometers. The location of each site is also labeled by a solid circle below the horizontal axis with lines connecting to respective site on overlying map. The horizontal scales of overlying digital topographic map and space-time diagram are the same. The vertical bars and upward pointing arrows at each study site reflect radiocarbon ages that bracket the age of surface in calendar years A.D. or B.C. (2σ standard deviation of the ^{14}C calendar ages). The vertically pointing arrows above some sites indicate the brackets encompass only the uncertainty of the youngest radiocarbon age in displaced deposits and thus the upper bound of the age of the last earthquake displacement may be younger (see text for discussion). The coseismic slip (*cs*), vertical separation (*vs*), and horizontal shortening (*hs*) of the corresponding earthquake are also shown in meters. The rupture extents of known large to great earthquakes within the study area are provided as a long box with the year of the rupture annotated within. Inferred rupture length is based on revised and expanded Medvedev-Sponheuer-Karnik (MSK) intensity [*Ambraseys and Bilham*, 2000; *Ambraseys and Jackson*, 2003; *Ambraseys and Douglas*, 2004; *Bilham*, 1995; *Bilham*, 2004; *Bilham and Ambraseys*, 2005; *Chander*, 1989; *Molnar and Pandey*, 1989; *Pandey and Molnar*, 1988; *Wallace et al.*, 2005]. Long bold and solid horizontal lines without ages annotated are speculated rupture lengths of earthquakes in ~A.D. 1100 and ~A.D. 1500 resulting from interpretation of timing and size of surface displacements observed in trench exposures (dotted where inferred in absence of paleoseismic data). Details and possible correlation of the event (bar) at ~A.D. 1500 with the historically documented 1505 event of *Ambraseys and Douglas* [2004] are further discussed in text.

Nepal (Figure 12). Our presentation of the results of paleoseismic investigations at three additional sites further to the northeast along the HFT within the Indian states of West Bengal and Assam extends the spatial coverage another ~500 km to the east. We combine the observations presented here with the earlier published results [*Kumar et al.*, 2001; *Kumar et al.*, 2006; *Lavé et al.*, 2005; *Nakata et al.*, 1998; *Upreti et al.*, 2000; *Yule et al.*, 2006] in the space-time diagram of Figure 12 that depicts (1) the distribution of strong ground shaking from historical earthquakes, (2) the temporal limits of past surface rupture events at each site based on radiocarbon ages from paleoseismic trenches, and (3) estimates of fault displacement recorded in the trench exposures at each site. It is this diagram that forms the basis of discussion.

[25] The extent of the thick horizontal bars labeled with the year of occurrence in the space-time diagram (Figure 12) delineate the distances along the arc subject to strong ground shaking during historical earthquakes. The shaded areas with a bold or bold dotted outline in the overlying map approximate the spatial coverage of ground shaking for the respective earthquakes. The solid horizontal bars in Figure 12 lacking annotations for age represent the speculative age and extent of ruptures interpreted from observations of the timing and amount of offset observed at trench sites along the arc. The extent of the interpreted ruptures and their temporal relationship to the historical record of ruptures gleaned from intensity data are the subject of the following discussion.

[26] Large historical earthquakes along the arc, from west to east, include the 1555 M_w ~ 7.6 Kashmir, the 1905 M_w ~ 7.8 Kangra, the 1803 M_w ~ 7.5 Kumaon-Garhwal, the 1505 Central Himalayan, the 1934 M_w ~ 8.1 Bihar, and the 1950 M_w ~ 8.4 Assam earthquakes [*Ambraseys and Bilham*, 2000; *Ambraseys and Jackson*, 2003; *Ambraseys and Douglas*, 2004; *Bilham*, 2004; *Bilham and Ambraseys*, 2005; *Chander*, 1989; *Pandey and Molnar*, 1988; *Wallace et al.*, 2005]. Knowledge of the earthquakes is generally based on interpretation of historical accounts of ground shaking. None of the earthquakes are known to be associated with accounts of surface rupture.

[27] In our earlier work, *Kumar et al.* [2001] and *Kumar et al.* [2006], we reported observations of the HFT to fold and break late Holocene near surficial sediments from a half a dozen trenches located between and at the boundaries of the 1905 and 1505 meizoseismal zones and across the zone of strong shaking interpreted for the 1803 event (Figure 12, sites 1–3, 5, and 6). As encountered in this study, geologic relationships and scatter in ages associated with disseminated detrital charcoal generally allowed only the definition of maximum bounding ages of fault displacements at each of the five sites. The maximum bounding ages at the five sites generally fall between about A.D. 1200 and 1400 (Figure 12). In addition to the absence of historical accounts of surface rupture, recent studies tend to argue that the 1905 earthquake was likely of insufficient size to produce surface rupture on the Himalayan front [*Ambraseys and Bilham*, 2000; *Wallace et al.*, 2005]. As well, the 1905 event appears to be located to the northeast of site 1. The 1 September 1803 M_w ~ 7.5 Kumaon-Garhwal earthquake is inferred to have ruptured approximately ~200 km in the vicinity of sites 5 and 6 based on sparse damage reports from the hilly terrain of the Himalayan-Garhwal region [*Ambraseys and Jackson*, 2003; *Ambraseys and Douglas*, 2004]. The displacement recorded in the trenches of sites 3, 5, and 6 are interpreted to be on the order of 16 to 26 m, significantly larger than would be expected from the interpreted size of the 1803 event. Complexities of exposure precluded clear estimates of the amount of coseismic displacement during the most recent surface rupture at sites 1 and 2. The large coseismic offsets suggested at sites 3, 5, and 6 are in greater accord with what would be expected from the size and length of the M_w ~ 8.2 1505 Central Himalayan earthquake, though the sites do fall to the west of the extent of the 1505 meizoseismal zone reported by *Ambraseys and Jackson* [2003] and *Ambraseys and Douglas* [2004], as shown in Figure 12. Given that the historical accounts are perhaps spatially incomplete and that the large displacements at sites 3, 5, and 6 might be due to the 1505 earthquake, the combined historical and paleo-earthquake data would suggest a lateral rupture extent on the order of ~700 km or greater (see *Kumar et al.* [2001, 2006] for detailed discussion).

[28] Farther to the east in Nepal, the study of *Lavé et al.* [2005] reports a surface rupture event displaying on the order of 17 m of coseismic offset and stratigraphic relationships to place the age of the event very close to A.D. 1100 (Figure 12, site Y). *Nakata et al.* [1998] and *Upreti et al.* [2000] report in abstracts a large surface rupture event constrained between the ages of A.D. 1050 and 1300 from a site several hundred kilometers to the east (Figure 12, site Z). Neither of the sites show evidence of displacement that may be attributed to the M_w 8.1 1934 Bihar-Nepal earthquake. In light of the large offset recorded at site Y, it is reasonable to speculate that displacements at sites Y and Z reflect the same earthquake. Our sites (Figure 12, sites A, B, and C) are east of sites Y and Z. Limits on the ages of surface rupture at Chalsa (site A) and Nameri (site B), though not tight, allow that the two sites record the same rupture as recorded at sites Y and Z in Nepal. If true, the rupture length of the event would approach 700 to 800 km. The speculation is motivated by the similarity in large displacements recorded at Chalsa (>14 m) and Nameri (>12 m) as compared to site Y in Nepal. Such large displacements are comparable to ~12 m, ~19 m, and ~20 m average dip-slip displacements calculated for the great 1964 Alaska earthquake (M_w 9.2), the 1960 Southern Chile earthquake (M_w 9.5), and the 2004 Indonesia/Andaman earthquake [*Park et al.*, 2005; *Sykes and Quittmeyer*, 1981]. The final and easternmost site C is characterized by a relatively much smaller offset of <2.5 m, temporal constraints that clearly place it after A.D. 1100, and a location at the edges of the 1950 Assam earthquake meizoseismal area. The possibility arises that the 1950 M_w 8.4 Assam earthquake may have produced the small offset recorded at site C.

[29] In summary, the results reported here extend paleoseismic coverage to ~1700 km along the Himalayan arc. The data are recognizably few in relationship to the length of the arc covered but are beginning to give a hint of the past history of surface ruptures along the arc. Likewise, the problem of detrital charcoal leading to a wide scatter in ages, the thin to absent nature of colluvial deposits associated with the young displacements, and the lack of deposits capping faulted units within the trenches generally have not allowed placement of upper age limits to the timing of the last earthquakes at most sites. Nonetheless, it seems that the data now define a boundary in western Nepal between two large

earthquakes that occurred in A.D. 1505 and A.D. 1100. And though constraints on the ages of surface ruptures at sites to the east and west of this boundary are not conclusive, the large offsets recorded at sites on both sides of the boundary and the tectonic context of offsets argue for the likelihood of rupture extents reaching upwards of 700 to 800 km along the arc. The prior work of *Kumar et al.* [2006] suggests that such large earthquakes as these can be expected to repeat on the order of every 1000 to 3000 years.

[30] **Acknowledgments.** This is CNS (Center for Neotectonic Studies) contribution 55. This work was conducted under National Science Foundation (NSF) grant EAR-0609556 with the support of both the NSF Tectonics and the Africa, Near East, and South Asia Program in the office of International Science and Engineering Programs. S.K. thanks travel support extended for fieldwork by the Division of Mechanical Sciences, Indian Institute of Science, during various stages of this work. R.J. thanks WIHG, Dehradun, for travel support to carry out this work. Authors thank officials of West Bengal and Assam forest departments for realizing the importance of the research and permitting us to place trenches within the reserved forest areas. We thank Goodricke Group Limited and the manager of the Harmutty Tea Estate for permitting us to place two trenches within their tea estate premises. This paper benefitted from insightful edits and comments by Rodolfo Console, Robert Yeats, Jayne Bormann, and an anonymous reviewer.

References

Acharyya, S. K., et al. (1986), Regional geology and tectonic setting of northeast India and adjoining region, *Mem. Geol. Surv. India*, *119*, 6–12.

Ambraseys, N., and R. Bilham (2000), A note on the Kangra M_s = 7.8 earthquake of 4 April 1905, *Curr. Sci.*, *79*(1), 45–50.

Ambraseys, N., and J. Douglas (2004), Magnitude calibration of north Indian earthquakes, *Geophys. J. Int.*, *159*, 165–206.

Ambraseys, N., and D. Jackson (2003), A note on early earthquakes in northern India and southern Tibet, *Curr. Sci.*, *84*(4), 571–582.

Avouac, J. P., and P. Tapponnier (1993), Kinematic model of active deformation in central Asia, *Geophys. Res. Lett.*, *20*(10), 895–898.

Banerjee, P., and R. Bürgmann (2002), Convergence across the northwest Himalaya from GPS measurements, *Geophys. Res. Lett.*, *29*(13), 1652, doi:10.1029/2002GL015184.

Bilham, R. (1995), Location and magnitude of the 1833 Nepal earthquake and its relation to the rupture zones of contiguous great Himalayan earthquakes, *Curr. Sci.*, *69*(2), 155–187.

Bilham, R. (2004), Earthquakes in India and the Himalaya: Tectonics, geodesy and history, *Ann. Geophys.*, *47*(2–3), 839–858.

Bilham, R., and N. Ambraseys (2005), Apparent Himalayan slip deficit from the summation of seismic moments for Himalayan earthquakes, 1500–2000, *Curr. Sci.*, *88*(10), 1658–1663.

Bilham, R., et al. (1997), GPS measurements of present day convergence across the Nepal Himalaya, *Nature*, *386*, 61–64.

Bilham, R., et al. (1998), Geodetic constraints on the translation and deformation of India: Implications for future great Himalayan earthquakes, *Curr. Sci.*, *74*(3), 213–229.

Chander, R. (1989), Southern limits of major earthquake ruptures along the Himalaya between 15 deg. E and 90 deg. E, *Tectonophysics*, *170*, 115–123.

DeMets, C., et al. (1994), Effect of recent revisions to the geomagnetic reversal time scale on estimates of current plate motions, *Geophys. Res. Lett.*, *21*, 2191–2194.

Gansser, A. (1964), *Geology of the Himalayas*, 289 pp., Wiley Intersci., London.

Gansser, A. (1983), *Geology of the Bhutan Himalaya*, 181 pp., Birkhäuser, Basel, Switzerland.

Harrison, T. M., et al. (1992), Raising Tibet, *Science*, *255*, 1663–1670.

Hussain, A., et al. (2008), Geological setting of the 8 October 2005 Kashmir earthquake, *J. Seismol.*, *13*, 315–325, doi:10.1007/s10950-008-9101-7.

Kondo, H., et al. (2008), Long recurrence interval of faulting beyond the 2005 Kashmir earthquake around the northwestern margin of the Indo-Asian collision zone, *Geology*, *36*(9), 731–734.

Kumar, S., et al. (2001), Earthquake recurrence and rupture dynamics of Himalayan Frontal Thrust, India, *Science*, *294*(5550), 2328–2331.

Kumar, S., et al. (2006), Paleoseismic evidence of great surface-rupture earthquakes along the Indian Himalaya, *J. Geophys. Res.*, *111*, B03304, doi:10.1029/2004JB003309.

Larson, K. M., et al. (1999), Kinematics of the India-Eurasia collision zone from GPS measurements, *J. Geophys. Res.*, *104*, 1077–1093.

Lavé, J., and J. P. Avouac (2000), Active folding of fluvial terraces across the Siwaliks Hills, Himalayas of central Nepal, *J. Geophys. Res.* , *105*(B3), 5735–5770.

Lavé, J., et al. (2005), Evidence for a great medieval earthquake (~1100 A.D.) in the Central Himalayas, Nepal, *Science*, *307*, 1302-1305.

Le Fort, P. (1975), Himalaya: the collided range: Present knowledge of the continental arc, *Am. J. Sci.*, *275A*, 1–44.

Malik, J. N., and T. Nakata (2003), Active faults and related Late Quaternary deformation along the northwestern Himalayan Frontal Zone, India, *Ann. Geophys.*, *46*, 917–936.

Martin, S., and W. Szeliga (2010), A catalog of felt intensity data for 570 earthquakes in India from 1636 to 2009, *Bull. Seismol. Soc. Am.*, *100*(2), 562–569.

Molnar, P., and M. R. Pandey (1989), Rupture zones of great earthquakes in the Himalaya region, *Earth Planet. Sci.*, *98*, 61–70.

Molnar, P., and P. Tapponnier (1975), Cenozoic tectonics of Asia: Effects of a continental collision, *Science*, *189*, 419–426.

Nakata, T. (1972), Geomorphic history and crustal movements of the foothills of the Himalayas, *Sci. Rep. Tohoku Univ., Ser. 7*, *22*, 39–177.

Nakata, T. (1989), Active faults of the Himalaya of India and Nepal, in *Tectonics of the Western Himalayas*, edited by L. L. Malinconico Jr. and R. J. Lillie, pp. 243–264, Geol. Soc. of Am., Boulder, Colo.

Nakata, T., et al. (1998), First successful paleoseismic trench study on active faults in the Himalaya, *Eos Trans. AGU*, *79*(45), Fall Meet Suppl., Abstract S22A-18.

Nelson, K. D. (1998), The Himalaya and Tibetan Plateau: A perspective from project INDEPTH, paper presented at 1998 Annual Meeting, Geol. Soc. of Am., Boulder, Colo.

Nelson, K. D., et al. (1996), Partially molten middle crust beneath southern Tibet: Synthesis of project INDEPTH results, *Science*, *274*(5293), 1684–1688.

Oatney, E. M., et al. (2001), Contribution of Trans-Yamuna active fault systems towards hanging wall strain released above the décollement, Himalayan foothills of northwestern India, *Himalayan Geol.*, *22*(2), 9–28.

Pandey, M. R., and P. Molnar (1988), The distribution of intensity of the Bihar-Nepal earthquake of 15 January 1934 and bounds on the extent of the rupture zone, *J. Geol. Soc. Nepal*, *5*, 22–44.

Pandey, M. R., et al. (1995), Interseismic strain accumulation on the Himalayan crustal ramp (Nepal), *Geophys. Res. Lett.*, *22*, 751–754.

Park, J. K., et al. (2005), Global Seismographic Network records the great Sumatra-Andaman earthquake, *Eos Trans. AGU*, *86*(57), 60–61.

Patriat, P., and J. Achache (1984), India-Eurasia collision chronology has implications for crustal shortening and driving mechanism of plates, *Nature*, *311*, 615–621.

Paul, J., et al. (2001), The motion and active deformation of India, *Geophys. Res. Lett.*, *28*, 647–650.

Reimer, P. J., et al. (2004), IntCal04 terrestrial radiocarbon age calibration, 0–26 cal kyr BP, *Radiocarbon*, *46*(3), 1029–1059.

Schelling, D., and K. Arita (1991), Thrust tectonics, crustal shortening, and the structure of the far-eastern Nepal Himalaya, *Tectonics*, *10*(5), 851–862.

Seeber, L., and J. Armbruster (1981), Great detachment earthquakes along the Himalayan Arc and long-term forecasting, in *Earthquake Prediction*: *An International Review*, *Maurice Ewing Ser.*, vol. 4, edited by D. W. Simpson and P. G. Richards, pp. 259–277, AGU, Washington, D. C.

Stuiver, M., and H. A. Polach (1977), Discussion; reporting of ^{14}C data, *Radiocarbon*, *19*(3), 355–363.

Stuiver, M., and P. J. Reimer (1993), Extended (super 14) C data base and revised CALIB 3.0 (super 14) C age calibration program, *Radiocarbon*, *35*(1), 215–230.

Sykes, L. R., and R. C. Quittmeyer (1981), Repeat times of great earthquakes along simple plate boundaries, in *Earthquake Prediction: An International Review*, *Maurice Ewing Ser.*, vol. 4, edited by D. W. Simpson and P. G. Richards, pp. 217–247, AGU, Washington, D. C.

Szeliga, W., et al. (2010), Intensity, magnitude, location, and attenuation in India for felt earthquakes since 1762, *Bull. Seismol. Soc. Am.*, *100*(2), 570–584.

Tapponnier, P., et al. (2001), Oblique stepwise rise and growth of the Tibet plateau, *Science*, *294*(5547), 1671–1677.

Treloar, P. J., and M. P. Coward (1991), Indian Plate motion and shape: Constraints on the geometry of the Himalayan orogen, *Tectonophysics*, *191*, 189–198.

Upreti, B. N., et al. (2000), The latest active faulting in Southeast Nepal, paper presented at Proceedings Active Fault Research for the New Millenium, Hokudan Int. Symp. and Sch. on Active Faulting, Awaji Island, Hyogo, Japan.

Valdiya, K. S. (1992), The Main Boundary Thrust zone of the Himalaya, India, *Ann. Tecton.*, *6*, 54–84.

Wallace, K., et al. (2005), Surface deformation in the region of the 1905 Kangra M_w = 7.8 earthquake in the period 1846–2001, *Geophys. Res. Lett.*, L15307, doi:10.1029/2005GL022906.

Wang, Q., et al. (2001), Present-day crustal deformation in China constrained by global positioning system measurements, *Science*, *294*, 574–577.

Wesnousky, S. G., et al. (1999), Uplift and convergence along the Himalayan Frontal Thrust of India, *Tectonics*, *18*(6), 967–976.

Yeats, R. S., et al. (1992), The Himalayan frontal fault system, *Ann. Tecton.*, *6*, S85–S98.

Yule, D., et al. (2006), Possible evidence for surface rupture of the Main Frontal Thrust during the great 1505 Himalayan earthquake, far-western Nepal, *Eos Trans. AGU*, *87*(52), Fall Meet. Suppl., Abstract S33C-05.

Zhao, W., et al. (1993), Deep seismic reflection evidence for continental underthrusting beneath southern Tibet, *Nature*, *366*, 557–559.

R. Jayangondaperumal, Wadia Institute of Himalayan Geology, Dehradun, 248001, Uttaranchal, India.

Y. Kumahara, Faculty of Education, Gunma University, 4-2, Aramaki, Maebashi, Gunma, 371-8510, Japan.

S. Kumar, Centre for Earth Sciences, Indian Institute of Science, Bangalore, 560012, India.

T. Nakata, Department of Geography, Hiroshima Institute of Technology, 2-1-1, Miyake, Saeki-ku, Hiroshima, 731-5193, Japan.

V. Singh, Department of Geology, Center for Advanced Study, Chhatra Marg, University of Delhi, Delhi 110007, India.

S. G. Wesnousky, Center for Neotectonic Studies, University of Nevada, Reno, MS 169, Reno, NV 89557, USA.